Energy Conversion and Management: X 24 (2024) 100733

Contents lists available at ScienceDirect

Energy Conversion and Management: X

journal homepage: www.sciencedirect.com/journal/energy-conversion-and-management-x

Optimal mixture design for organic Rankine cycle using machine learning algorithm

Valerio Mariani [a], Saverio Ottaviano [b,*], Davide Scampamorte [b], Andrea De Pascale [b], Giulio Cazzoli [a], Lisa Branchini [b], Gian Marco Bianchi [a]

[a] Group "Development and Simulation of Low-impact Internal Combustion Engines", Department of Industrial Engineering, University of Bologna, viale del Risorgimento 2, 40136 Bologna, Italy

[b] Group "Fluid Machines and Energy Systems", Department of Industrial Engineering, University of Bologna, viale del Risorgimento 2, 40136 Bologna, Italy

A B S T R A C T

This study presents a new design tool for working fluid mixtures in organic Rankine cycles. The proposed tool comprises a blend model for the thermophysical properties of the formulated mixtures, an ORC model to predict the performance of the mixtures in a specific application, and an optimizer based on the Bayesian inference method to identify the optimal mixtures compositions to be assessed. The tool is programmed to optimize an objective function based on predefined optimization targets. Importantly, the targets and their respective weights within the objective function can be adjusted to meet the specific requirements of the application under analysis, making this approach adaptable to diverse research and industrial objectives. The algorithm is applied to a case study to demonstrate its ability to define a low-GWP blend that can replace HFC-134a in a micro-scale ORC with recuperator, while maintaining and potentially enhancing performance. The optimization targets specified for the case study are the net power output, the net efficiency, the GWP and the blend size. Power and efficiency are computed through a validated model of the low-temperature ORC system used as benchmark case. The results showed that the procedure was able to formulate several blends that comply with the targets of the assigned task. Amongst the high-scoring mixtures, the most used pure fluids are R32, R152a, R1234yf, and R1234ze(E). The presence of HCs is limited to fewer mixtures, playing the main role of GWP-limiter. A method to estimate the flammability classification of the blends has been also applied, obtaining that most of them belong to the ASHRAE class 2l, except when an HC is present, in which case the fluid is may result in class 3.

1. Introduction

Organic Rankine cycle (ORC) is considered a mature technology in the field of low-grade heat-to-power conversion. However, there is still substantial potential for further commercial deployment, as a large amount of heat from renewable sources (e.g., geothermal and solar energy) and waste heat remains underutilized. Currently, the total installed capacity worldwide is around 4.5 GW, with future market growth mainly expected in geothermal and small waste heat applications [1,2]. The main obstacles to widespread adoption are related to economic and performance issues, such as high installation costs and relatively low conversion efficiency, leading to long payback periods. The performance of the system is strongly affected by the working fluid, whose selection represents a critical aspect influencing the efficiency and applicability of ORC systems [3].

Traditional organic fluids, such as refrigerants and hydrocarbons (HC), have been predominantly used due to their favourable thermodynamic properties. However, emerging concerns regarding environmental impact, safety, and efficiency have propelled the exploration of alternative working fluids. Among these alternatives, the use of mixtures as working fluids in the ORC has garnered considerable attention. Mixtures offer the potential to tailor fluid properties to match specific application requirements, such as target values of thermodynamic properties or environmental impact [4]. By blending different pure molecules, it is possible to achieve desirable characteristics, including improved heat transfer, enhanced thermal stability, and reduced undesired properties, such as flammability or Global Warming Potential (GWP). Zeotropic mixtures may improve cycle performance due to their ability to match the temperature profiles of heat sources more closely and to reduce the exergy losses during non-isothermal phase change [5,6]. Furthermore, there is a growing need to replace high-GWP substances, which can be addressed by blending them with low-GWP fluids, particularly during the transition to environmentally cleaner solutions. Several works have been dedicated to demonstrating the potential benefits of the adoption of ORC fluid blends, in terms of performance improvement, greater sustainability, and safety issues. For example, Braimakis et al. [7] investigated the exergetic performance of binary mixtures of R32 and ultralow-GWP fluids in ORCs, finding that zeotropic mixtures enhance efficiency, especially at lower heat source

* Corresponding author.
E-mail address: saverio.ottaviano2@unibo.it (S. Ottaviano).

https://doi.org/10.1016/j.ecmx.2024.100733
Received 16 July 2024; Received in revised form 24 September 2024; Accepted 25 September 2024
Available online 29 September 2024

Nomenclature

Acronyms

BS	Blend size
BWR	Back Work Ratio
GP	Gaussian Process
GWP	Global Warming Potential
HC	Hydrocarbon
HFC	Hydrofluorocarbon
HFO	Hydrofluoroolefin
HoV	Heat of Vaporization (kJ/kg)
MW	Molar weight (kg/kmol)
OPT	Mixture with the highest objective function score
ORC	Organic Rankine Cycle
UCB	Upper Confidence Bound

Symbols

A	Acquisition function
c_P, c_V	Specific heat at constant pressure and volume (kJ/kg/K)
D	Searching domain (pure fluids of the fluid list)
F	Number of atoms of fluorine
F_{obj}	Objective function
H	Number of atoms of hydrogen
h	Specific enthalpy (kJ/kg)
K	Kernel matrix
$\dot{m}_{ORC}$	ORC mass flow rate (g/s)
M	Predictive mean function; Mixture
N	Normal distribution; Rotating speed (rpm)
p	Pressure (bar)
P_{net}	Net power production (W)
$\dot{Q}$	Thermal power (W)
T	Temperature (°C) or (K)
$\dot{V}$	Flow rate (l/s)
w	Weight of the objective function
X	Input domain values (mass fraction)

Subscript

ad	Adiabatic flame (referred to the temperature)
amb	Ambient (referred to the temperature)
BS	Minimum blend size (referred to individual optimal mixture)
C,in	Cold water inlet at condenser
CR	Critical (referred to the temperature)
ev	Evaporator
exp	Expander
GWP	Minimum GWP (referred to individual optimal mixture)
H,in	Hot water inlet at the evaporator
L	Saturated liquid state
P	Maximum net power output (referred to individual optimal mixture)
pp	Pump
ref	Reference state
sat	Saturation
V	Saturated vapor state
η	Maximum net efficiency (referred to individual optimal mixture)

Greek letters

β	Expansion ratio (−)
η_{net}	Net efficiency (−)
θ	Exploration/exploitation split hyperparameter
λ	Thermal conductivity (W/m/K)
μ	Dynamic viscosity (Pa·s)
ρ	Density (kg/m^3)
σ	Molecular complexity (kJ/kg/K^2)

temperatures. Shu et al. [8] assessed the utilization of highly flammable HC blended with flammable retardants (such as R11 and R123) to obtain low-GWP mixtures and, at the same time, mitigate the resulting flammability.

In the literature, the working fluid optimization has been addressed in numerous studies. On the highest level, the optimization task can be classified in three categories, depending on the solution domain considered, as follows:

- **Optimization within a list of defined conventional fluids**: this approach involves selecting from a predefined set of conventional fluids available in thermodynamic libraries. The optimization process typically utilizes established properties of these fluids to find the most suitable candidate for specific applications, such as efficiency and environmental impact in ORCs.
- **Optimization considering the design of new molecules:** this method focuses on the design of entirely new molecules using Computer-Aided Molecular Design (CAMD) models. It employs computational techniques to generate novel molecular structures with tailored properties, optimizing them based on performance metrics relevant to their intended application. This approach allows for the exploration of previously unconsidered chemical species.
- **Optimization by mixing conventional fluids:** this technique involves creating mixtures of two or more conventional fluids to enhance performance characteristics. By optimizing the composition of these mixtures, it is possible to achieve desired thermodynamic properties that may not be attainable with single-component fluids. This method can be particularly useful in achieving specific performance or environmental goals while maintaining compatibility with existing systems.

Regarding the optimization techniques used in the working fluid selection process, the most adopted methods fall into three main categories, namely deterministic, heuristic, and statistical optimization, whose main features are summarized in Table 1. In the following, a non-exhaustive state of the art review is presented with relevant examples for each of the optimization techniques.

An example of **deterministic** technique applied to conventional fluids can be found in Freeman et al. [12], which presents a fluid optimization problem in a domestic-scale distributed solar combined heat and power (S-CHP) system based on ORC engine. They compared eleven pure fluids of different families (HFC, HCFC, CFC, HC) over a wide range of evaporation temperatures (between 60 °C and 240 °C). The fluids that emerged from the parametric optimization considering different irradiance levels are R245ca, R123, R11, however, new low-GWP working fluids that might have been suitable for the application, such as the hydrofluoroolefin (HFO) R1234yf or R1233zd, were not included.

Chen et al. [15] presented a study on the design of ORC working fluids by combining the group contribution method (GCM) with cubic equations of state for calculating thermophysical properties. By fixing the operating conditions, the optimization process aims to maximize the output work by means of parametric optimization. The optimal fluid, resulting from the parametric optimization of subcritical cycle, is CH2FCF2CF3, with an evaporation temperature of 113 °C, a net power output of 276 kW, and an efficiency close to 12 %.

Schilling et al. [14] presented a method for the integrated design of ORC cycle and working fluid mixture using a 1-stage CoMT-CAMD

Table 1
Main optimization techniques.

	Deterministic [9]	Heuristic [10]	Statistical [11]
Definition	Deterministic optimization methods yield repeatable results for well-defined problems based on fixed input values. The outcomes are entirely predictable, as there is no randomness involved in the process.	Heuristic optimization methods search for satisfactory solutions through rules of thumb or trial-and-error approaches. They do not guarantee optimality but provide good enough solutions in a reasonable timeframe.	Stochastic optimization incorporates randomness into the optimization process, acknowledging that some parameters may be uncertain or variable. This approach aims to find robust solutions that perform well under various scenarios.
Characteristic	**Exact Solutions**: Provides optimal ad hoc solutions under defined constraints by means of fine tuning. **Predictability**: The same inputs will always produce the same outputs.	**Speed**: Generally faster than deterministic methods. **Flexibility**: Can be applied to a wide range of problems without extensive modification.	**Handling Uncertainty**: Effectively deals with variability in data or model parameters. **Probabilistic Models**: Often uses statistical methods to inform decision-making.
Examples	Linear programming, nonlinear programming, and parametric optimization.	Genetic algorithms, simulated annealing, particle swarm optimization, and neural networks.	Stochastic gradient descent, Monte Carlo methods, and Bayesian optimization.
Example references	[12 13 14 15 16 17]	[18 19 20 21 22]	[23]

approach. They applied this method to a small-scale ORC for low-temperature waste heat recovery application, employing the PC-SAFT to model both equilibrium and transport properties of mixtures. They used mixed-integer nonlinear program (MINLP) as optimization technique. The binary mixture propane/diethyl ether resulted the optimal solution in terms of net power output, while the blend propene/propionaldehyde ensured the lowest specific investment cost.

Cignitti et al. [16] utilized an integrated working fluid/plant optimization approach to optimize the waste heat recovery of the exhaust gas from a marine diesel engine. Their tool combines CAMD technique with deterministic optimization of the cycle key parameters such as net power output, pressure ratio, and degree of superheating. Best-performing fluids were 2,2,3,3,4,4,5,5-octafluorohexane and 5-chloro-4,5,5-trifluoro-2,3-dimethylpent-2-ene, which both offer improved cycle performance and a low environmental impact.

Also White et al. [13] employed a deterministic method (MINLP), and extended the CAMD model to the design of blends of working fluids for non-recuperated subcritical ORC systems. They identified isoheptane, 2-pentene, and 2-heptene as optimal solutions for heat-source temperatures of 150 °C, 250 °C, and 350 °C, respectively, with specific investment costs (SICs) of £5620, £2760, and £2070 per kW, and power outputs of 33 kW, 137 kW, and 214 kW.

With regards to **heuristic** techniques, Chitgar et al. [19] evaluated three geothermal-based ORC configurations to optimize energy production for freshwater generation and minimize the total cost rate, utilizing a multi-objective optimization technique that combines genetic algorithms (GA) and artificial neural networks (ANN) to model system. They achieved the highest exergy efficiency with R1233zd(E) at vaporization temperature of 135 °C, while R1234ze(Z) offered the lowest total cost rate. Ammonia was identified as the best overall choice for maximizing power generation and freshwater production, demonstrating superior performance in terms of levelized costs of electricity.

The heuristic approach was also used by Papadopoulos et al. [20], who developed a CAMD methodology that employs group contribution methods in combination with simulated annealing (SA) multi-objective optimization for the generation of optimum working fluid. They applied their method to a representative example of ORC supplied by low temperature heat source (below 100 °C), obtaining best energetic and economic performance with methyl-formate and methoxy-ethane due to their favorable balance of efficiency, low flammability, toxicity, and minimal environmental impact. Another example is available in Lampe et al. [18], where the authors optimized both the working fluid and process parameters using the continuous-molecular targeting (CoMT-CAMD) approach. The optimization employs the perturbed chain statistical associating fluid theory (PC-SAFT) model to evaluate thermophysical properties, with the net power output as the unique objective. They identified a list of ten most promising working fluids – including HFCs, HCFCs and HCs – with a power output ranging between 1.6 and 2.7 MW, for the low-temperature geothermal application under consideration.

Li et al. [22] applied another heuristic technique – namely the Particle Swarming Optimization (PSO) – to design low-GWP refrigerant mixtures for HVAC system, with the aim of maximizing energy efficiency and minimizing flammability. They identified R32/R1234yf and R32/R1234yf/R125 as best-performing mixtures, obtaining an improvement of cycle efficiency and a significant reduction of flammability and GWP compared to the benchmark case.

Fang et al. [21] utilized a genetic algorithm for multi-objective optimization of a non-recuperated ORC system that recovers heat from the exhaust gas of a heavy duty diesel engine. They considered four working fluids (R245fa, R123, toluene and decane) and their zeotropic mixtures, and varied the evaporation and condensation temperatures over a wide range, finding that zeotropic mixtures are able to reduce heat transfer area but leading to lower thermodynamic performances.

Heuristic methods, such as those mentioned hereabove, simplify the searching process, and offer fast search capabilities while ensuring a solution of sufficient quality. However, they may fall short in finding the global optimum solution and lack clear measures of result quality across all potential options. On the other hand, deterministic optimization provides precision and predictability, but it is computationally intensive and lacks of flexibility, hence it may result more effective in problems that feature a small-size solution domain.

In this context, **statistical** (or stochastic) techniques emerge as attractive options. Statistical methods can combine some pros of both deterministic and heuristics techniques, such as the achievement of optimal solutions and flexibility to the problem definition, ensuring also a low computational effort. Specifically, Bayesian optimization, leveraging a probabilistic surrogate model and an acquisition function based on Bayes' theorem [24], stands out for its ability to efficiently map the solution domain. The strength of this method lies in i) the possibility to approach unknown black-box objective functions of any complexity without special requirements on their derivatives; ii) the ability to provide information on both the predicted shape of the objective function and its uncertainty by means of the statistical nature of the surrogate function; iii) the efficient drawing of the objective function in multi-dimensional domains by means of the acquisition function; iv) the capacity of achieving the global optimum. The state of the art analysis reveals that, despite their potential, the use of statistical methods for ORC working fluid design has been minimally explored, with only a few recent studies available. A relevant example can be found in the work published by Díaz-Secades et al. [23], where the Bayesian approach is applied to the optimization of the ORC working fluid in a marine waste heat recovery system. Among 80 pure substances they considered, the low-GWP fluids R1233zd(E), Novec 649 and SES36 presented the highest performance, with a maximum power recovered around 160 kW.

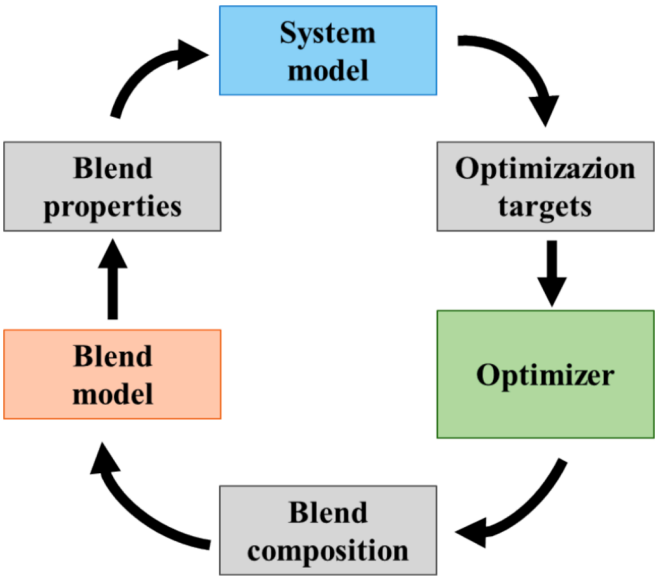

Fig. 1. General structure of the optimization tool.

1.1. Aim and contribution

This work focuses on developing an optimization tool based on Bayesian inference, aiming to guide the identification of low-GWP fluid mixtures for ORC applications. The tool integrates a validated ORC model and a set of simple equations for assessing the thermal properties of the formulated mixtures. To demonstrate the methodology's capabilities, the code was executed for the task of replacing R134a in a low-temperature micro-ORC with a new mixture, aiming to enhance performance and reduce environmental impact. This case study has been chosen primarily due to the availability of a validated ORC model, thanks to the test bench installed in the UNIBO laboratory [25]. Nonetheless, we believe the case study is significant as the system can be employed with several low-temperature heat sources in small applications, such as low-grade waste heat recovery, geothermal and solar thermal energy. Nonetheless, the procedure can be employed for any fluid design task, by changing some input parameters and variables and the optimization targets and implementing a specific ORC model if required. An extensive discussion is dedicated to the analysis of the optimal mixtures, providing the reader with potential post-processing techniques to assess the results reliability. The main contributions of the study are summarized as follows:

- Utilization of Bayesian statistical method for optimizing ORC fluid mixtures. To our knowledge, in the literature this technique has been adopted only by [23] for the optimization of pure fluids, while mixtures so far have been mostly designed by means of deterministic and heuristic approach. Thus, this work is one of the first to show the high potential of Bayesian optimisation tools to guide the definition and production of market mixtures of fluids.
- ORC model validated within the benchmark case included in the optimization algorithm, and methodology to adjust the empirical coefficients accounting for the change of fluid.
- Low information and tuning requirements for the tool, enabling it to provide useful results even in the early stages of the design process.
- Modular structure of the tool, allowing for the integration or replacement of different function blocks to target diverse objectives.

The search algorithm is a modified version of the original work by some of the authors [26], as well as the ORC model, which is adapted from the one presented in [27]. A preliminary version of the procedure has been presented in [28], where a simplified version of the blend model was introduced. The main developments since that study include the integration of the ORC model into the optimization routine, improvement to the objective function and targets with corresponding weights and normalisation techniques, and the application of a method for estimating the safety classification of formulated mixtures.

2. Materials and methods

The general structure of the procedure is the one described in Fig. 1, and is made essentially of three blocks of functions. The algorithm is developed with the aim of being modular, allowing the users to implement their libraries or tools just by replacing one or more corresponding blocks. The tool can be employed for the first design of a system as well as in the case of retrofitting an existing plant. Moreover, it can be targeted for diverse specific purposes at different stages of a project.

Following the scheme of Fig. 1, the general features of the main functions are reported below, while the detailed description of the approach is presented in sections 2.1–2.3 for the case study analysed in this work. In this work, each module has been developed in Python.

The blend model is any system of rules used to calculate the thermal and transport properties of the formulated mixture. It must comprehend, at least, the equations of state (EoS) for all the pure fluids to be mixed. In the application presented here, a hybrid approach is implemented with the open-source library CoolProp used to compute pure fluids' properties, which are then inserted into user-defined expressions for the mixtures' properties.

The system model contains the functions for computing the performance of the mixture in the specific application. It can involve a detailed model of the ORC heat exchangers and machines, if available, or a simpler one with constant parameters based on the conditions of the heat source and sink. This stage is the one associated with the highest uncertainty contribution, since even a validated model may be inaccurate if the working fluid changes. This aspect should also be accounted for when choosing the pure fluids to be mixed. Here, a previously developed and validated semi-empirical model of a micro-ORC system is used [27].

The optimizer represents the actual optimization tool, used for combining the given pure fluids in a certain number of blends depending on the user-defined objective function, by learning from previous iterations. In this study, the optimizer is based on the Bayesian probabilistic approach.

The setup presented in the following sections is specifically related to a possible application of the tool, i.e. the replacement of a high-GWP hydrofluorocarbon (HFC) in a plant retrofit with new low-GWP mixtures. Different applications can be considered: for example, in a simpler version of the algorithm [28], the target was to optimize a low-GWP mixture with similar properties to those of R134a, without considering a specific application or working conditions. In that case, the system model was not included in the procedure, as the fluid properties were available from the blend model and fed directly to the optimizer block.

2.1. Blend model

A set of rules and correlations has been defined for the assessment of the blends' thermal and transport properties. The properties are required to solve the equations in the ORC model and are used as points of comparison between the mixture solutions.

The blend model is based on the knowledge of the thermophysical properties of the pure fluids composing the mixture. For this task, the open-source library CoolProp V6.4.3 [29] has been employed.

The rules have been established pursuing three defined goals: i) good accuracy over a certain range of conditions; ii) low computation time (i.e. iterative routines must be limited); iii) being mostly based on mathematical laws, avoiding the use of empirical coefficient. The implementation of rules against the use of well-established codes, such as REFPROP, has been adopted for three main reasons: i) the choice to

Table 2
Expressions of the mixing rules adopted in the blend model.

Property	Rule
Critical temperature	$T_{CR} = \sum x_i T_{CR,i}$
Enthalpy	$h = \sum z_i h_i$
Heat of vaporization	$HoV = \sum z_i HoV_i$
Heat capacities	$c_{P/V} = \sum z_i c_{P/V,i}$
Thermal conductivity	$\lambda = \sum z_i \lambda_i$
Global Warming Potential	$GWP = \sum z_i GWP_i$
Density	$\frac{1}{\rho} = \sum \frac{z_i}{\rho_i}$
Viscosity	$\ln\mu = \sum x_i \ln\mu_i$
Molecular complexity	$\sigma = \frac{s_{Tr} - s_0}{0.7T_{CR} - T_0}$

develop an open source and fully editable tool, thus, licensed software with pre-defined list of fluids should be avoided; ii) the need of quick calls for mixture properties calculation, as a slowing down of the Python code due to REFPROP calls has been experienced; iii) feeding REFPROP with complex mixtures that are not included in its fluid list may cause properties extrapolation out of the reliability range, increasing the uncertainty associated with such properties. This issue has been discovered also in other works [15].

Accordingly, the following set of rules has been selected as blend model: i) the mixture's critical temperature (T_{CR}) is calculated as moles weighted average; ii) the mixture's enthalpy (h), heat of vaporization (HoV), heat capacities (c_P,c_V), thermal conductivity (λ), and GWP values are calculated as mass weighted averages; iii) the mixture's density (ρ) is calculated as mass weighted inverse average; iv) the dynamic viscosity (μ) is calculated according to the Grunberg-Nissan law [30]. The expression has been simplified by neglecting the cross terms that involve empirical coefficients, which may not be available for all the fluids; v) the quality of the expansion (dry, wet or isentropic) is quantified by the so called molecular complexity (σ), defined as the inverse of the slope of the saturated vapor line calculated by definition at reduced temperature $T_r = 0.7 \cdot T_{CR}$; vi) the saturation temperatures (T_{sat}) and pressures (p_{sat}) are calculated by solving the Vapor-Liquid Equilibrium (VLE) for non-ideal mixtures via the Soave-Kwong-Redlich equation of state. The full expressions for the calculation of properties from critical temperature to molecular complexity are summarized in Table 2.

For addressing the VLE problem, the system of equations reported in Eq. (1) is implemented and numerically solved. The system comprises the VLE for each non-ideal component (x and y are the mass fractions of vapor and liquid phase, respectively), the calculation of the fugacity coefficient, Φ, the Soave-Kwong-Redlich (SKR) cubic equation of state [31] (with Z compressibility factor), and the mass conservation. α, β, A, and B are fluid-dependent parameters. The complete description of this approach is presented in [26].

$$\begin{cases} y_i \cdot \Phi_i^V \cdot p = x_i \cdot \Phi_i^L \cdot p \\ \Phi_i = exp\left[\beta_i(Z-1) - ln(Z-1) - \frac{A}{B}(\alpha_i - \beta_i) \cdot ln\left(1 + \frac{B}{Z}\right)\right] \\ Z^3 - Z^2 + (A - B - B^2) \cdot Z - AB = 0 \\ \sum_{i=1}^{N} x_i = 1 \end{cases} \quad (1)$$

All the rules included in the blend model have been validated by comparing the resulting properties with those of a set of 53 commercial mixtures [32], calculated using REFPROP as a benchmark. For the validation of temperature- and pressure-dependent properties, four reference states have been selected, characterized by temperatures equal to 20 °C and 70 °C, and vapour quality equal to 0 (saturated liquid) and 1 (saturated dry vapor). The validation results have shown that the properties calculated via the user-defined expressions feature a coefficient of determination (R^2) greater than 0.9 in all the four test conditions. Only for the expression used for the viscosity of the saturated liquid, a slightly under-performance is observed, which however ensures $R^2 > 0.8$. The extensive validation results are provided as parity plots in the Appendix.

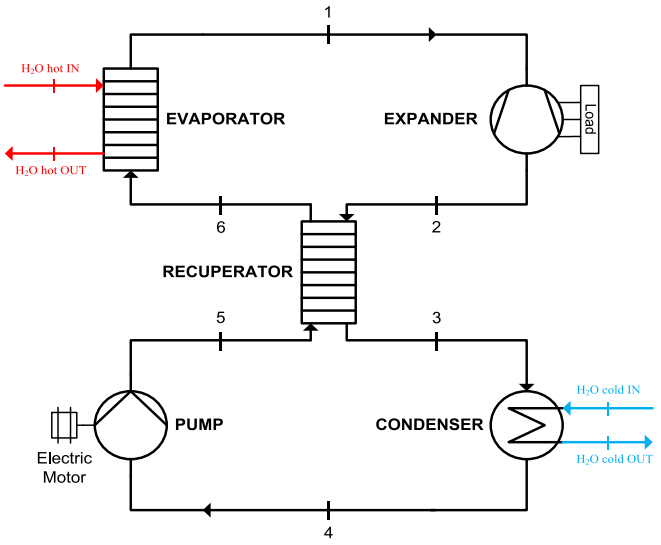

Fig. 2. Simplified Micro-ORC test bench layout.

2.2. ORC model

The cycle model implemented in the procedure is derived from the one presented in [27], related to the micro-ORC test bench installed at the University of Bologna.

The system is a recuperated ORC using HFC-134a as working fluid. The nominal power output is around 2 kW, while the temperature of the heat source ranges between 50 °C and 90 °C. It is driven by a volumetric piston expander with three radial cylinders. A simplified version of the ORC layout is presented in Fig. 2. In the regular operation, the working fluid in the liquid state is drawn by the pump, then it is preheated in the recuperator before entering the evaporator, where it is vaporized and superheated at high pressure. The vapor is expanded in a piston expander, leading to the reduction of its temperature and pressure while remaining in the vapor state. In the recuperator, the low-pressure vapour transfers the residual sensible heat to the evaporator-inlet liquid stream. After the recuperator, the exhaust vapor is condensed in the condenser to restart the cycle. Liquid water is used as hot source and cold sink is water. For the full description of the test bench, its components and the control equipment, please refer to [25,33].

Fig. 3 reports the workflow diagram of the ORC model, which is formed by the combination of the sub-models of each of the main components. The code is developed in Python 3.0 using the *numpy* and *scipy* open libraries. Each component of the system has been implemented as a Python function and included in a two-level implicit problem, thus, the solution is reached through an iterative process on two iterative control variables: the expander inlet temperature (T_1) and the condenser outlet temperature (T_4).

The input variables are the flow rates and temperature of the hot source and cold sink at the inlet of the evaporator ($\dot{V}_{H,in}$, $T_{H,in}$) and condenser ($\dot{V}_{C,in}$, $T_{C,in}$), and the ambient temperature (T_{amb}). The outputs are the thermodynamic state of all the sections indicated in Fig. 2, the thermal power transferred in the heat exchangers and the electrical power of pump and expander. The solution is achieved iteratively by reducing the errors on the two iterative variables, T_1 and T_4. The model was calibrated using experimental data acquired with R134a as working fluid, with temperatures of the heat source ranging from 60 to 85 °C and

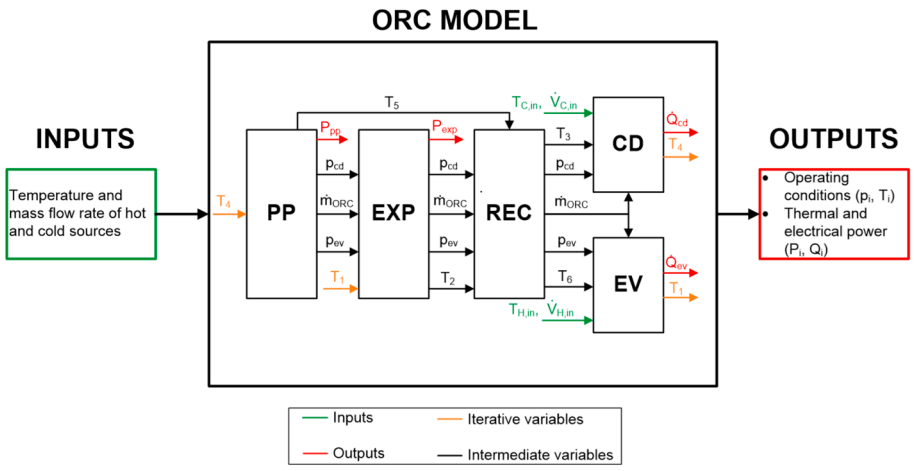

Fig. 3. Workflow diagram of the ORC model. The inputs are shown in green, the iterative variables are shown in orange, the intermediate variables are shown in black, the output are shown in red. (For interpretation of the references to colour in this figure legend, the reader is referred to the web version of this article.)

with a range of expander power output between 200 and 1600 W.

More in detail, the **heat exchangers** (evaporator, recuperator, condenser) are modelled with the ε–NTU method and a moving boundary approach applied in steady-state conditions. According to this method, evaporator and condenser are split into three heat transfer regions (subcooled zone, two phase zone and superheated zone). The global heat power ($\dot{Q}_{HE}$) is calculated by the sum of the heat transfer occurring in the i-th zone, according to Eq. (2):

$$\dot{Q}_{HE} = \sum \dot{Q}_i = \sum \dot{Q}_{max,i} \cdot \varepsilon_i \tag{2}$$

where $\dot{Q}_i$ is the real power exchanged in the i-th zone and $\dot{Q}_{max,i}$ is the related ideal power, according to the well-known definition of heat transfer effectiveness ε_i. The latter is determined for the evaporator and the recuperator via Eq. (3), valid for plate heat exchangers (the form for the shell-and-tube condenser is omitted for the sake of brevity) [34]. The subscript i indicating the difference zone is omitted for better readability.

$$\varepsilon = \frac{1 - e^{-\frac{UA}{C_{min}}\cdot\left(1-\frac{C_{min}}{C_{max}}\right)}}{1 - \frac{C_{min}}{C_{max}}\cdot e^{-\frac{UA}{C_{min}}\cdot\left(1-\frac{C_{min}}{C_{max}}\right)}} \tag{3}$$

with C_{min} and C_{max} corresponding to the minimum and maximum thermal capacity of the hot and cold fluid, U is the global heat transfer coefficient, calculated with common correlations for the estimation of convective coefficients [35], and A is the heat exchanger surface area, which is a calibration parameter. According to the procedure applied in [27], the value of U is adjusted accounting for the change of fluid properties with respect to the benchmark case (R134a), in particular the density ρ, the specific heat c_p, the thermal conductivity λ and the viscosity μ, by means of Eq. (4).

$$U_{fluid} = U_{R134a} \cdot \left(\frac{\rho_{fluid}}{\rho_{R134a}}\right)^{0.8} \cdot \left(\frac{c_{p_{fluid}}}{c_{p_{R134a}}}\right)^{\alpha} \cdot \left(\frac{\lambda_{fluid}}{\lambda_{R134a}}\right)^{1-\alpha} \cdot \left(\frac{\mu_{R134a}}{\mu_{fluid}}\right)^{0.8-\alpha} \tag{4}$$

with coefficient α assumed equal to 0.4, 0.3 and 0.35 for the evaporator, the condenser and the recuperator respectively [36]. For the complete treatment of the calculation procedure, please refer to [27].

The **expander** model is the one introduced in [37], adapted from the semi-empirical method developed for volumetric expanders in [38] and [36]. The approach provides for solving the ideal internal expansion as the combination of an isentropic expansion and an isochoric pressure drop. The resulting ideal power is then diminished by the various losses contributions, which include recompression, under- or over-expansion, pressure losses at the intake and discharge valves, internal leakages and heat dissipation to the ambient. The expander power output and total efficiency are then calculated according to Eq. (5) and Eq. (6), where η_{em} represents the electro-mechanical efficiency of expander and generator.

$$P_{exp} = (h_1 - h_2) \cdot \eta_{em} \tag{5}$$

$$\eta_{exp} = \frac{P_{exp}}{h_1 - h_{2,is}} \tag{6}$$

The expansion model is well-represented by the scheme in Fig. 4,

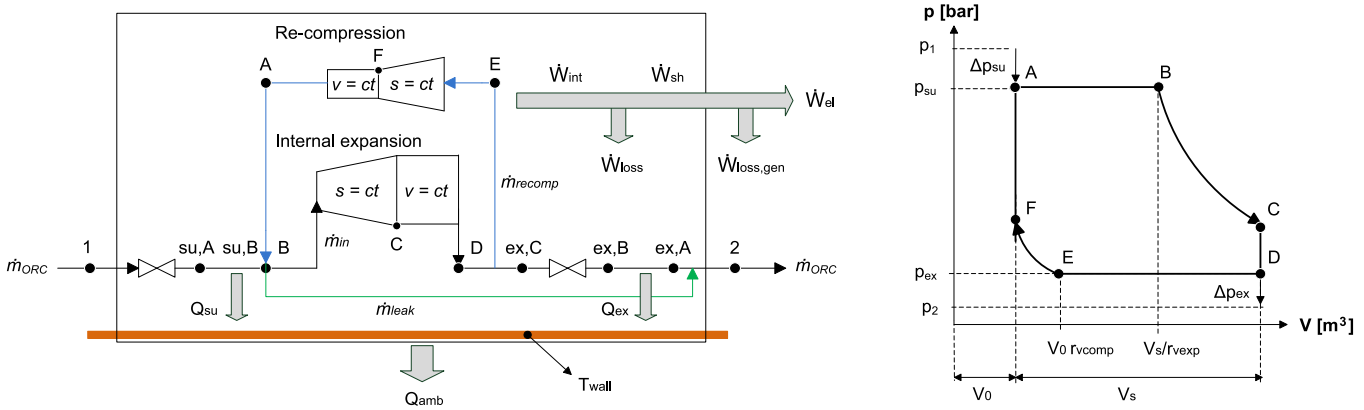

Fig. 4. Volumetric expander sub-model scheme and p-V diagram.

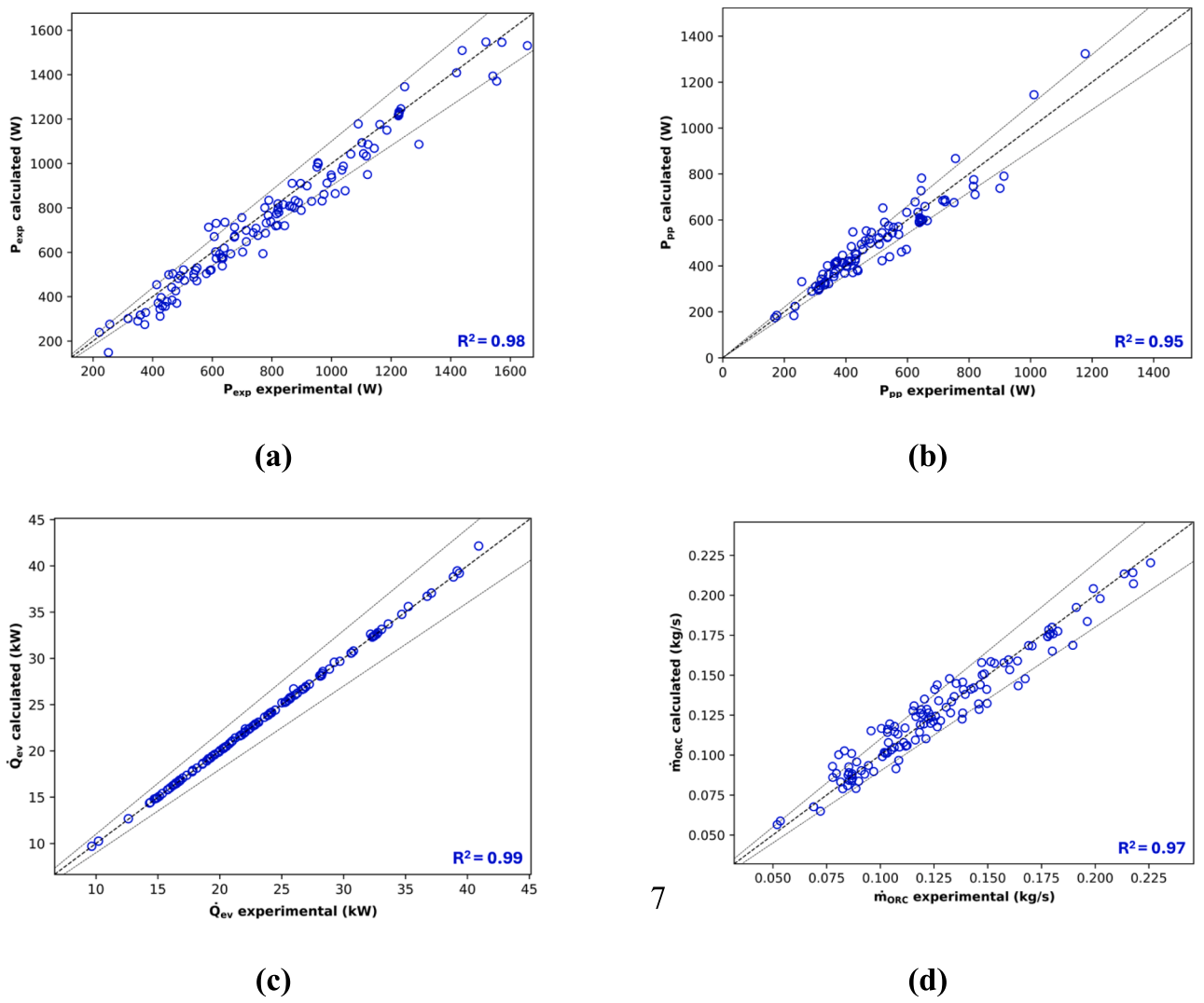

Fig. 5. Parity plot between experimental and calculated: a) Expander power production, b) Pump power absorption, c) Evaporator heat power absorption, d) mass flow rate. The error band is set at 10%.

which also reports a generic pressure–volume diagram of the piston expander. The extended explanation of the model can be found in [37,27].

The **feed-pump and circuit resistance** model is used to calculate the pressure increase, Δp, and the volumetric flow rate, $\dot{V}$. It is based on the characteristic curve obtained experimentally with the benchmark fluid, and modified for each formulated mixtures using correlations that involves fluid-dependent variables, such as density and viscosity [27]. The pump's electric power consumption is determined by its efficiency, η_{pp}, which accounts for both hydro-mechanical and electromechanical losses. The value of η_{pp} is calibrated with experimental data [27].

$$P_{pp} = \frac{\dot{V} \cdot \Delta p}{\eta_{pp}} \tag{7}$$

The overall performance is determined by assessing the net power output ($P_{net} = P_{exp} - P_{pp}$) and net efficiency ($\eta_{net} = \frac{P_{net}}{\dot{Q}_{ev}}$), which are included among the optimization targets within the case study discussed hereinafter.

The validation results are shown in Fig. 5 only for the main performance indicators (expander and pump power, evaporator power and mass flow rate), in a wide range of operating conditions.

2.3. Optimizer

The optimization algorithm is based on the Bayesian statistical inference, which aims at finding the optimum across the solution domain by combining exploitation and conscious exploration. The algorithm is inspired by a previous work of some of the authors [26], in which the Bayesian approach is applied to maximize the match between gasolines of unknown composition from the market and multicomponent mixtures from the optimizer.

The role of the optimization algorithm is to get intel on the shape of objective function (F_{obj}) across the input domain (D) using the minimum number of evaluations. Based on this iteratively increased knowledge, the algorithm eventually identifies the set of input values that returns the global maximum value of the objective function.

According to the conditional probability definition, the Bayesian statistics provides a routine to review the belief on how the mixture composition shapes the objective function once new evidences are given from the latest composition test. In the first step, no information on the objective function are available, thus, a training set of the input values is used (typically by a uniformly distributed random selection) to evaluate the associated value of the objective function. This sampling is then used to create the so called 'priors', i.e. the initial beliefs on the shape of the function, namely the surrogate function. The typical choice for the

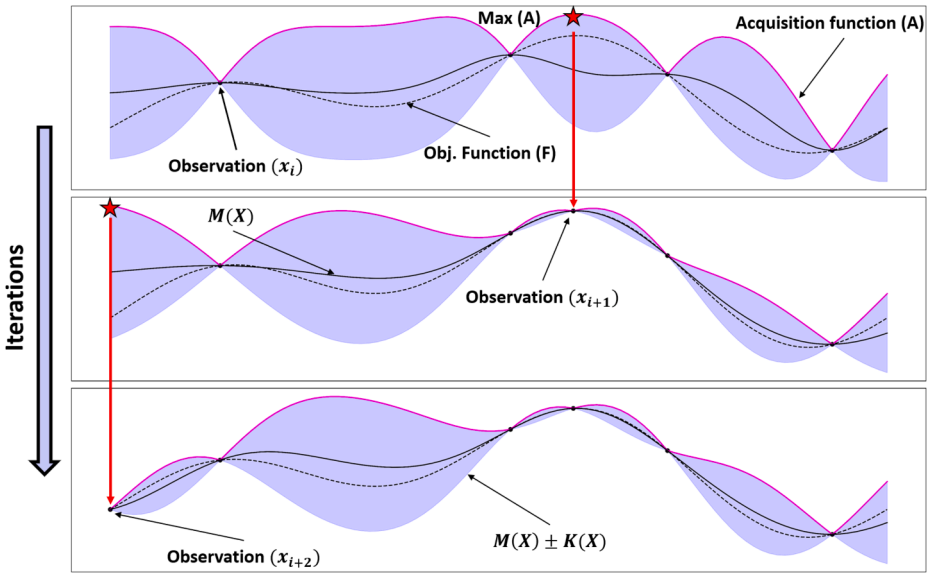

Fig. 6. Illustration of three iterations of the Bayesian iterative routine including the current observations (black dots), the predictive mean function (solid black line), the uncertainty including the set of likely fitting functions (blue area), the acquisition function (solid violet line), the new point to evaluate (red star). (For interpretation of the references to colour in this figure legend, the reader is referred to the web version of this article.)

surrogate function is the Gaussian Process (GP), which assumes that the possible values of the objective function in each point of the input values (X) domain are normally distributed $N \approx \pm 2$ std deviation). Therefore, in a multi-dimensional domain the GP 'prior') is a set of possible functions that fit the training set including the predictive mean function $M(X)$, which precisely interpolates the training set, and other functions that interpolates the values that are normal distributed ± 2 std deviation) around the mean of each test point. Those other functions are defined in shape by the kernel matrix $K(X)$.

$$GP(X) = N(M(X), K(X)) \tag{8}$$

Based on the shape of the priors, the next point to be evaluated must be selected, aiming at gathering from it as much as possible information on the objective. In order to accomplish this task, the Bayesian algorithm relies on the acquisition function ($A(X)$), i.e. a merit function which defines the sampling strategy by combining exploitation and conscious exploration. In this framework, exploiting means testing new solutions in the surroundings of a mapped zone of the input domain where good scores have been returned. Exploring means testing new solutions in zones of the input domain with poor information on the value of the objective function. In this study, the Upper Confidence Bound (UCB) acquisition function (Eq. (9)) is adopted due to its easy formulation, clear expression and control of the exploitation/exploration split, and ability to promote a faster convergence [39]. Thus, the new evaluation point will be the input set that maximizes $A(X)$. In Eq. (9), θ is the exploitation-exploration split hyperparameter. $\theta = 0$ means full exploitation, thus, new evaluations will be performed close to the latest maximum value of the predictive mean. High θ values (e.g. > 5) mean a heavy weight on the exploration phase, thus, new evaluations will be moved towards points associated to the maximum uncertainty of the GP priors (i.e., the bounding functions of the 95 % normal distribution).

$$A(X) = M(X) + \theta \cdot K(X) \tag{9}$$

At this step, the new point is evaluated, and the corresponding value of the objective function is used to update the priors. Thus, the GP is re-calculated including the new pairs (X, F) by means of the Bayes' theorem to generate the new set of fitting functions (again according to a multivariate normal distribution) called 'posteriors'. This process is repeated iteratively by using the posteriors of the former iteration as priors for the next one up to the maximum number of iterations fixed by the user.

Table 3
List of fluids for the optimization.

Fluid	Family	T_{CR}(K)	GWP 100 y [42]
R134a	HFC	374.2	1430
R32	HFC	351.3	675
R245fa	HFC	427.0	1030
R227ea	HFC	374.9	3580
R152a	HFC	386.4	124
Propane	HC	370	3
i-butane	HC	407.8	5
R1234yf	HFO	367.9	4
R1234ze(E)	HFO	382.5	6
R1233zd(E)	HFO	439.6	77

A graphical illustration of the steps of this routine is given in Fig. 6 for a one-dimensional example. In Fig. 6 the dotted black curve is the black-box objective function F, the solid black line is the predictive mean $M(X)$, the blue area bounds the y-range in which lie all the functions that can fit the actual observations, the violet line is the UCB acquisition function (a high θ value has been used in this example, thus, the next evaluation point (red star) is taken at the maximum uncertainty).

2.4. Algorithm set-up and convergence

The Bayesian optimization routine is developed in *Python 3.0* by means of the *bayes_opt* [40] and *numpy* open libraries. In this study, the searching domain D is represented by the mass fraction values of the pure fluids included in the fluid list (X). The mass fraction of each pure fluid is limited at 80 %, while the minimum threshold is imposed equal to 4 % in order to include only fluids that contribute significantly on the characteristics of the final mixture. The pure fluids embodied in the searching domain have been selected by means of a preliminary screening based on the following criteria: i) the fluid's thermophysical properties must be available (i.e. the fluid is included in the CoolProp library); ii) the fluid's critical temperature is around the value of T_{CR} related to the fluid that must be replaced (within a maximum range of $\pm$ 70 K); iii) fluids belonging to different chemical families are included; iv) fluids with non-null value of the Ozone Depletion Potential (ODP) are excluded; v) the number of fluids in the list should be limited to a maximum around 20, in order to maintain good performance of the

Table 4
Case–study data provided to the micro-ORC model for the optimization process.

Input	Value
T_{amb}	20 °C
$T_{H,in}$	75 °C
$T_{C,in}$	15 °C
$\dot{V}_{H,in}$	1.8 l/s
$\dot{V}_{C,in}$	1.4 l/s

Table 5
Hyperparameters definition.

Hyperparameter	Choice/Value
Optimization targets	Normalized
Random samples	50
Maximum iter	300
GP regressor kernel	Matérn
ν	5/2
α	1.0×10^{-6}
θ	0.5
GWP regularization	1.0
Weights (−)	
w − net power	0.25
w − net efficiency	0.35
w − GWP	0.10
w − BS	0.30

numerical method [41]. In the present case, the list of ten fluids presented in Table 3 has been selected as searching domain.

The nominal operating condition selected for the optimization is defined by the input data of the ORC model, which are provided in Table 4.

The performance of each mixture option is evaluated via the objective function F, whose general expression has been identified in the weighted average of four user-defined optimization targets. The weights w_i are hyperparameters associated to each optimization target. Adjusting the value of the weight means to change the importance assigned to the contribution given by the corresponding target to the final score of the mixture. In some cases, when the code is struggling to optimize a target, we may decide to increase its weight to rebalance its contribution to the objective function. As far as the weighted average is concerned, the sum of the weights must be unitary, thus, the chosen value of each weight lies in the interval 0–1.

The quantities selected as optimization targets are: the net power output P_{net} and the net efficiency η_{net} resulting from the operation of the ith mixture in the system model; the GWP of the blend; the 'blend size' (BS), namely the number of components in the mixture. The ratio behind this objective function shaping is the search of working fluids that can improve, or at least maintain, the performance of the existing plant (higher or equal power output and efficiency) while fulfilling the environmental constraint to be on market (limited GWP) and practical realization (limited number of components). Due to the different measure units and order of magnitudes of the target properties, each one has been normalized as follows: for net power production and net efficiency, the normalisation values are taken equal to the maximum values achieved experimentally in the reference system with the fluid R134a ($P_{net,ref}$, $\eta_{net,ref}$); GWP and BS are normalized against the lower limits of 150 (according to the latest limitations posed by the F-gas regulation [43]) and 4 (typical size of commercial mixtures), respectively. The final expression of the objective function is reported in Eq. (10).

$$F_{obj} = w_{P_{net}} \cdot \frac{P_{net}}{P_{net,ref}} + w_{\eta_{net}} \cdot \frac{\eta_{net}}{\eta_{net,ref}} + w_{BS} \cdot \frac{4}{BS} + w_{GWP} \cdot \frac{150}{GWP} \tag{10}$$

In this form, the right-hand side of Eq. (10) can be divided into two parts: i) the first half is composed of two performance terms, which contribute to higher scores if the normalisation value is exceeded. Thus, mixtures that outperform the R134a as working fluids (achievement of greater net power and net efficiency predicted by the ORC model) are rewarded. ii) the second half is composed of two constraints terms, which contribute to higher scores if they are below the normalisation value. Thus, mixtures with less than four components and GWP lower than 150 are rewarded.

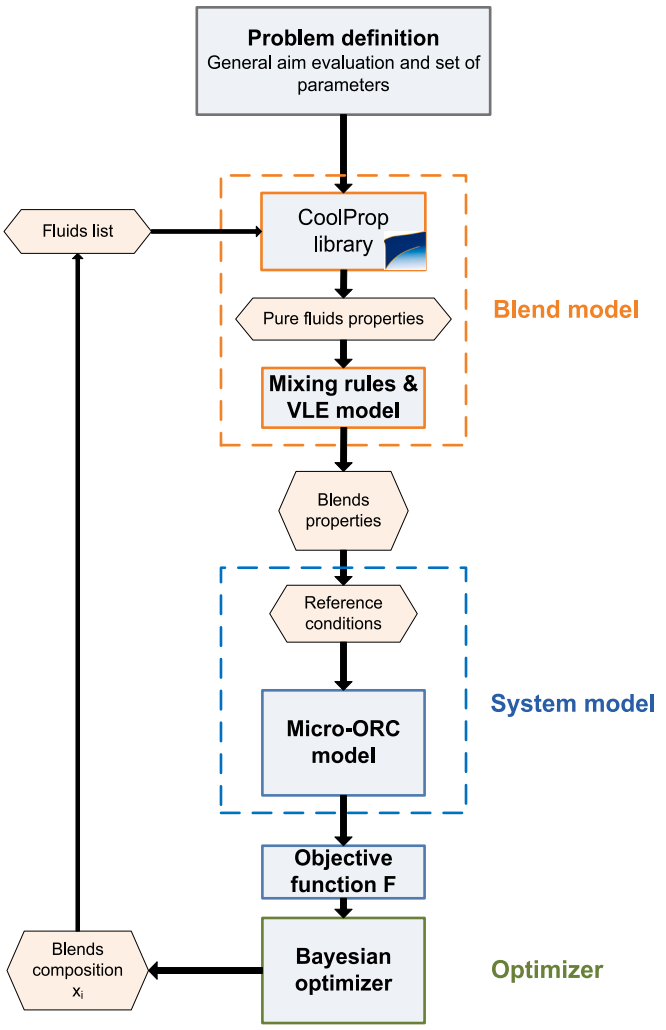

Fig. 7. Workflow of the optimization algorithm applied to the benchmark case.

For the sake of brevity, Eq. (10) can be summarized as $F_{obj} = F_P + F_\eta + F_{BS} + F^*_{GWP}$. The mark on the term F^*_{GWP} means that the contribution of the warming potential is regularized if the GWP value is lower than 150. This expedient is adopted to prevent the dominance of the F_{GWP} in case of mixtures with ultra-low GWP, which would mislead the search towards non-optimal solutions in terms of performance. In the state of the art, this principle is widely used in the framework of neural networks with L1 and L2 regularization techniques [44].

In Table 5 the hyperparameters of the algorithm and their values are summarized. The number of random samples, the number of maximum iterations, the exploitation-exploration split (θ) and the GWP regularization threshold, and the weights have been tuned, while the other hyperparameters are default of the library [40]. Both the random samples and the maximum iter have been set after different test runs.

Increasing the random samples enhances the likelihood of pointing solutions around the high objective zone of the domain, in order to provide the guided search with some high potential starts. Increasing the maximum iter gives the possibility to check that different successive scores are smaller, or at least in line, compared to higher ones obtained.

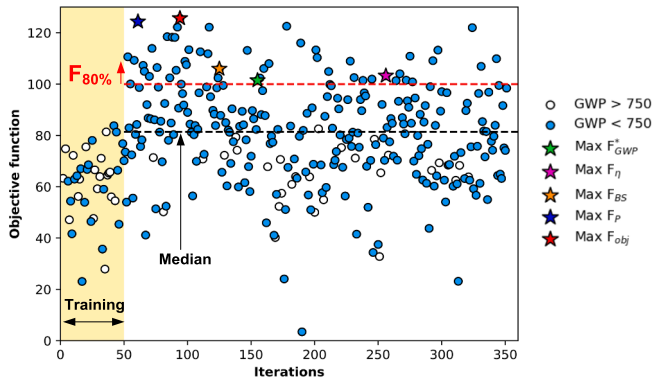

Fig. 8. Overall objective function score achieved during the optimization process. The black dashed line represents the median value of the objective function; light blue circles represent mixtures with GWP<750; white circles represent mixtures with GWP>750; the star marker represents best mixtures. (For interpretation of the references to colour in this figure legend, the reader is referred to the web version of this article.)

This would be a sign that both the refinement and the conscious exploration cannot detect new zones of the search domain that include outperforming solutions.

A trial-and-error approach has been applied in order to determine the maximum number of both random samples and iters as well as the value after which a further increasing would not significantly change neither the score nor the components' type/number associated to successive solution. The regularization threshold has been set aiming at equalizing the reward to solutions with GWP 150, thus, solutions with GWP=150 (compliance required by the marketplace) and GWP=4 contribute in the same manner to the final score. The weights have been tuned by starting from their uniform distribution (each weight equal to 0.25) and then increasing/decreasing their values according to the value achieved by the associated objective term (F_P, F_η, F_{BS}, F^*_{GWP}) against the overall score (F_{obj}). The goal was to avoid reaching high overall score given by the combination of excellent scores plus scarce scores of some of the objective terms. Therefore, starting from $w_i = 0.25$, the optimizer straggles to find solutions with efficiency higher than the reference working fluid as well as a number of components lower than six. Thus, the values of $w_{\eta_{net}}$ and w_{BS} have been arbitrarily increased. Then, in order to ensure the unity of the weights' sum (begin the objective function a weighted average), the values of $w_{P_{net}}$ and w_{GWP} should be decreased. As far as the optimizer can find solutions with extremely low GWP (e.g., 4), focusing the weight decrease only on the GWP term could be a balanced choice to avoid solutions without improved power (if $w_{P_{net}}$ would have been decreased as well) while ensuring compliant GWP despite the penalty introduced.

The workflow of the optimization algorithm is reported in Fig. 7.

Given that the optimizer operates on a statistical inference approach, executing multiple runs with identical parameters will yield different results each time. The overall convergence of the method should be assessed based on the consistency and reliability of the outcomes. During the post-processing phase, the algorithm convergence can be verified by comparing the composition of the high-scoring mixtures ($F_{80\%}$) across different runs (typically at least five). These mixtures should contain the same components with similar mass fractions and exhibit comparable values of the objective function. Additionally, the balance between the different contributions to F_{obj} can be examined, as will be elaborated in Section 3. If any of these aspects are found to be unsatisfactory, the convergence can be enhanced by adjusting the parameters of the objective function (such as the weights w_i), modifying the optimizer parameters (like the split hyperparameter θ), or increasing the number of iterations.

3. Case study results

Once the optimisation process has been completed, the results are subjected to two distinct analytical procedures. Initially, the algorithmic performance and the overall results are examined. Subsequently, the most relevant mixture solutions are analysed in greater detail, along with their performance in the case study.

3.1. Algorithm performance

Fig. 8 shows the overall distribution of the blend scores versus the iterations of a complete run, for a first evaluation of the general performance of the algorithm. At the end of the optimization process, the tool has designed 350 mixtures, of which the first 50 are obtained within the training phase and 300 are the trained solutions. Among these, 268 fulfil the light constraint of GWP<750, (light blue circles). The solutions associated to the maximization of each optimization target are marked with coloured stars. Considering only the trained iterations, 99 % of the objective function values lie in the range between 30 and 126, with a median around 81. Concerning only the training iterations, the median reaches the lower value of 63, and 94 % of their scores is below the median of the trained solutions, confirming the effectiveness of the learning process. As a further effect of the good training process, the optimizer starts to find high-score solutions at an early stage (17 % of optimization process). Then, the global optimum is reached at 27 % of the process (red star), but the code continues finding mixtures with total scores next to the highest until the last iterations. This behaviour is the consequence of the exploitation strategy of the Bayesian algorithm, as described in Section 2.3.

The following analyses will be focused on a subset of forty-nine high-score solutions characterized by values of objective function above 100, corresponding to 80 % of the maximum achieved score ($F_{80\%}$).

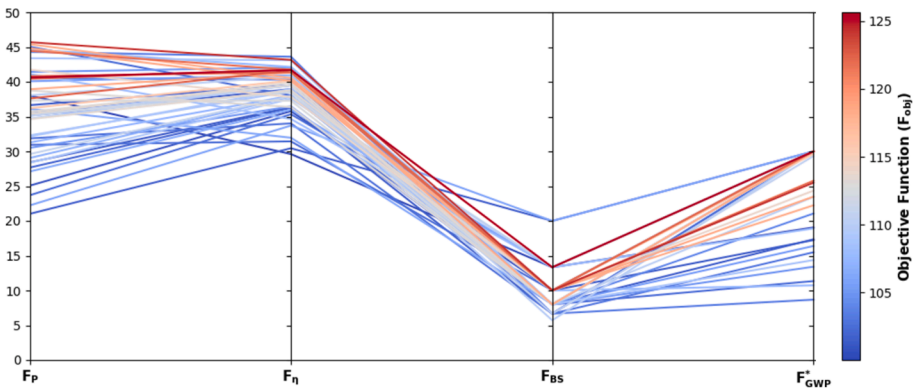

Fig. 9. Illustration of the value assumed by each optimization target for the most relevant solutions ($F_{80\%}$).

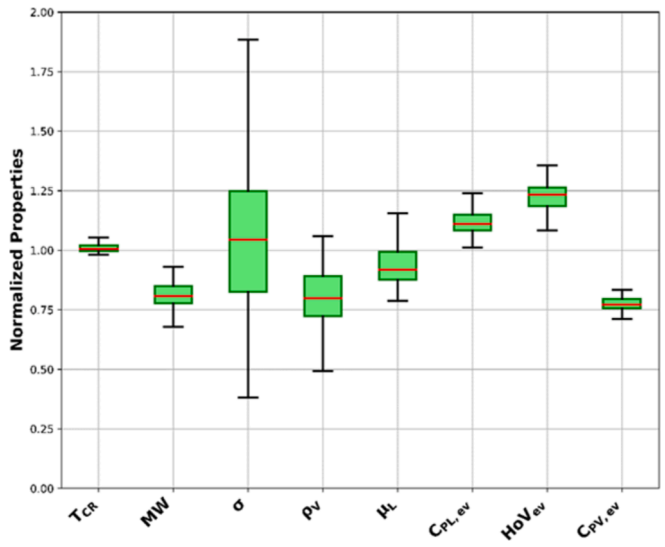

Fig. 10. Box chart of the main properties of interest for fluid selection in ORC cycle. The median value is shown with red line; the lower edge of the box represents the first quartile (Q1); the upper edge of the box represents the third quartile (Q3); The lines extending beyond the box stretch from the minimum value (Q1-1.5·IQR) to the maximum value (Q3 + 1.5·IQR) each variable can take. (For interpretation of the references to colour in this figure legend, the reader is referred to the web version of this article.)

For each of the 49 high-score mixtures, Fig. 9 reports the individual contribution of each weighted optimization target (F_P: net power; F_η: net efficiency; F_{BS}: blend size; F_{GWP}: GWP) in a parallel coordinates plot. Each line is one of the high-score mixtures, with the colour depicting the value of the objective function according to the colour scale provided on the right. Lines intercept the parallel axis at the value of the corresponding single weighted contribution to F_{obj}. Such plot is instrumental in illustrating the balance among the contributions of the optimization targets to the total score of each mixture.

Due to the form of the objective function and the weight values assigned to each optimization target (see Table 5), it is clear that the terms F_{BS} and F_{GWP} present a maximum that can be determined *a priori*, due to the regularization described in Section 2.4. In particular, the max F_{BS} equal to 20 is achieved with blends composed of two fluids, while the max F_{GWP} equal to 30 is obtained with any value of GWP lower than 150.

On the other hand, the maximum achievable values of F_P and F_η are higher and cannot be established *a priori*. As a consequence, the largest share of the total score F_{obj} is associated with the performance of the blend (power and efficiency). Moreover, the individual scores of power and efficiency present a quite balanced trend, especially within the blends with highest total score (dark and light red lines). The mixtures with highest scores present a BS between 3 and 5.

3.2. Mixture analysis

In order to perform a preliminary analysis of the designed mixtures in the micro-ORC virtual test bench, a statistical analysis is conducted on some key properties. The statistical analysis is presented in Fig. 10, in which the properties are presented as normalized values against the ones of the reference working fluid (R134a) in order to give a compact overview. All the properties present the median value around the ± 25 % and a narrow range of IQR (interquartile range), except for σ, ρ_V, and μ_L.

Critical temperatures are close to the R134a as a consequence of the pure fluids chosen to compose the database. Therefore, all the best mixtures exploit efficiently the low-grade heat source (hot source temperature lower than 100 °C) with a sub-critical cycle. The molecular weight of the full set of the considered solutions is below that of R134a. Molecular complexity of the solutions subset presents the widest range of IQR (0.42), beside the median value is closed on R134a. In the graph, normalized $\sigma < 1$ describes a lower superheated degree needed by some mixtures to avoid wet expansion. The maximum increase in slope is below −2.2, indicating that the solutions can be considered at least isentropic, as the R134a with a σ value of −1.2, as opposed to wet fluids like water with a much more pronounced negative slope (σ = -9.2). Vapor density presents a 20 % decrease in the median value, which says that for most of the designed mixtures a decrease of the refrigerant mass used in the system would be observed in working conditions, as well as a reduction of the expander production. Thus, a high rotational speed of the positive displacement must be considered for the improvement of the performance indexes. The viscosity of the designed mixture is a key parameter to check since a significant decrease suggests that the mixtures may suffer from larger working fluid leakage in the gear pump. In this case, μ_L presents a median value of 0.92 and an IQR of 0.12, thus, no relevant consequences are expected, otherwise, the change of the fluid machinery or other cautions should be considered. Enhanced thermal properties (normalized values > 1), such as latent heat and liquid specific heat at evaporator conditions, may result in a better heat absorption compared to R134a. This is likely a consequence of the zeotropic nature

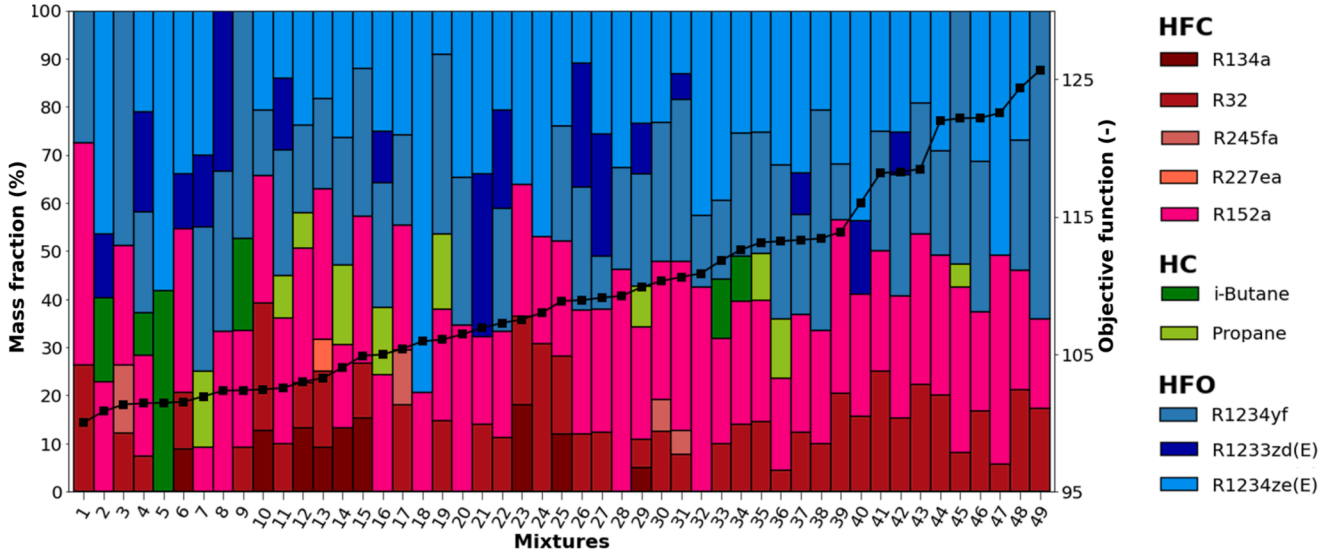

Fig. 11. Composition of the most relevant mixture solutions (left-hand axis), and the corresponding objective function score (black line, right hand axis).

Table 6
Composition and objective function score of individual optimal mixtures provided and main properties at 1 atm.

Mixture	Composition	Mass fraction (%)	F (−)	Fi (−)	ρ_L/ρ_V(kg/m^3)	μ_L/μ_V(μPa·s)	λ_L/λ_V(mW/m/K)	c_{PL}/c_{PV}(kJ/kg/K)	HoV(kJ/kg)
M_{GWP}	i-Butane / R1234ze(E)	42 / 58	101.46	F^*_{GWP} = 30	865.49/4.09	265.09/8.26	97.78/11.54	1.65/1.11	260.67
M_η	R134a / R32 / R1234yf /R227ea / R152a / R1234ze (E)	9 / 16 / 19 / 7 / 31 / 18	103.25	F_η = 43.6	1211.10/4.25	324.29/9.22	116.91/9.29	1.39/0.86	266.78
M_{BS}	R152a / R1234ze(E)	21 / 79	105.94	F_{BS} = 20	1225.60/5.01	326.47/9.28	98.06/10.01	1.35/0.85	222.73
M_P	R32 / R1234yf /R152a / R1234ze (E)	21 / 27 / 25 / 27	124.35	F_P = 30	1210.30/4.21	317.15/9.11	119.78/9.15	1.39/0.86	268.47
M_{OPT}	R32 / R1234yf / R152a	17 / 64 / 19	125.64	–	1218.50/4.54	302.31/8.98	110.03/8.99	1.33/0.84	246.37

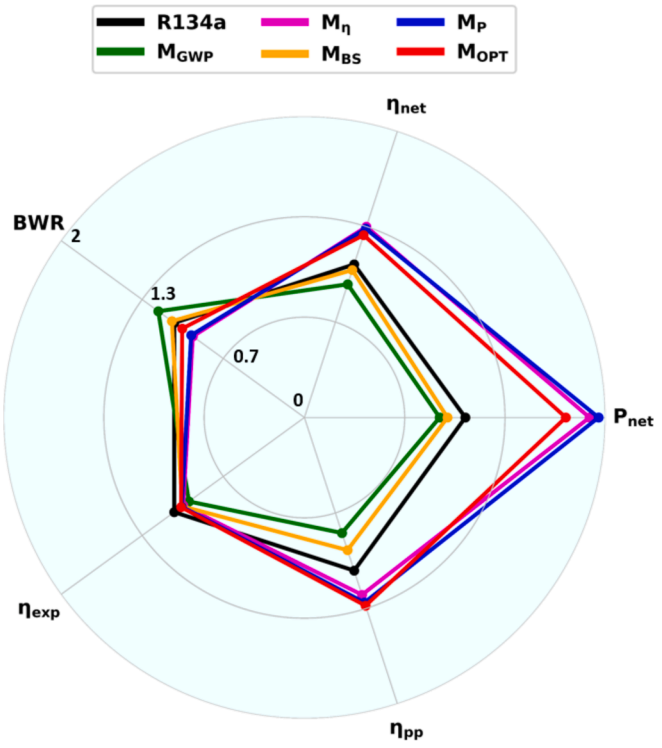

Fig. 12. Comparison between main performance indexes of the five ndividual optimal mixtures, against the R134a.

of most of the designed mixtures, that reduces the irreversibility during the heat exchange. Besides, a decrease of vapor specific heat can be noticed.

3.1.1. High-scoring mixtures ($F_{80\%}$)

Fig. 11 shows the composition of the high–score mixtures. The mixtures are sorted by increasing values of the objective function (black curve). In Fig. 11: it is visible that the most performing mixtures are mainly composed of HFOs and HFCs in similar proportions. Four pure fluids are recurrent in the designed mixture, namely R32, R152a, R1234yf, R1234ze(E). R1234yf and R1234ze(E) are the most employed HFOs due to their low-GWP (close to zero) and to their thermal properties that are similar to those of R134a. This result is consistent with the current state of the art, as these HFOs are the most employed working fluids for replacing the R134a [45].

Fluids like R245fa, R227ea, R134a are barely used moving towards the right side of the graph (i.e. high values of objective function), likely due to their high GWP. It is worth mentioning that R245fa is scarcely selected due to the presence of R1233zd(E), which is recognized as its 'clean' substitute. The latter is not selected frequently due to the high value of the critical temperature compared to the heat source temperature considered in this study, which negatively affects the ability of the mixture to take advantage of the heat source. The presence of HCs is limited to less mixtures with low mass fraction (14.8 % on average), playing the main role of GWP-limiter as their contribution to the performance targets is rather low.

3.1.2. Individual optimal mixtures

The analysis is now focused on the five solutions marked with stars in Fig. 8 (blend with lowest GWP (M_{GWP}), highest efficiency (M_η), minimum BS (M_{BS}), maximum net power production (M_P), maximum overall score (M_{OPT})), whose specifics are reported in Table 6 along with thermal properties calculated at 1 atm for liquid and vapor. It can be observed that values of liquid density (ρ_L) are similar (around 1220 kg/m^3) for all these mixtures, with the exception of M_{GWP} that presents a density 865 kg/m^3, which can be ascribed to the large presence of isobutane. The same applies to liquid viscosity (μ_L) that exhibits the lowest value for M_{GWP}. A different trend is observed for the specific heat, with is significantly higher for M_{GWP} both in liquid (1.65 kJ/kg/K) and vapor state (1.11 kJ/kg/K). Heat of vaporization of the five individual optimal blends is between 220 and 270 kJ/kg, with the lowest value for M_{BS} and the highest for M_η and M_P.

The radar chart in Fig. 12 compares the values of net power output (P_{net}), net efficiency (η_{net}), back work ratio (BWR), expander efficiency (η_{exp}) and pump efficiency (η_{pp}), calculated for the mixtures included in Table 6 and the reference fluid R134a, in the working conditions reported. The BWR corresponds to the ratio between the pump power

Table 7
Fluids performance indicators and operating conditions.

FLUIDS	$P_{net}(W)$	BWR(%)	η_{exp}(%)	η_{pump}(%)	$\dot{m}_{ORC}(g/s)$	$N_{pp}(rpm)$	$N_{exp}(rpm)$	$p_V(bar)$	$\beta(-)$
R134a	532.64	48.68	36.44	27.26	152.5	197.35	752.7	18.16	2.52
M_{GWP}	447.73	54.65	32.33	20.56	111.82	177.55	1717.46	11.97	3.03
M_η	943.93	41.72	33.93	31.57	178.66	257.7	1300.74	19.85	2.82
M_{BS}	473.57	49.54	34.21	23.62	130.35	179.55	963.14	14.58	2.79
M_P	973.59	42.33	34.33	32.94	187	274.8	1296.68	20.98	2.77
M_{OPT}	865.32	45.72	34.52	33.5	190.43	290.25	1075.89	21.48	2.75

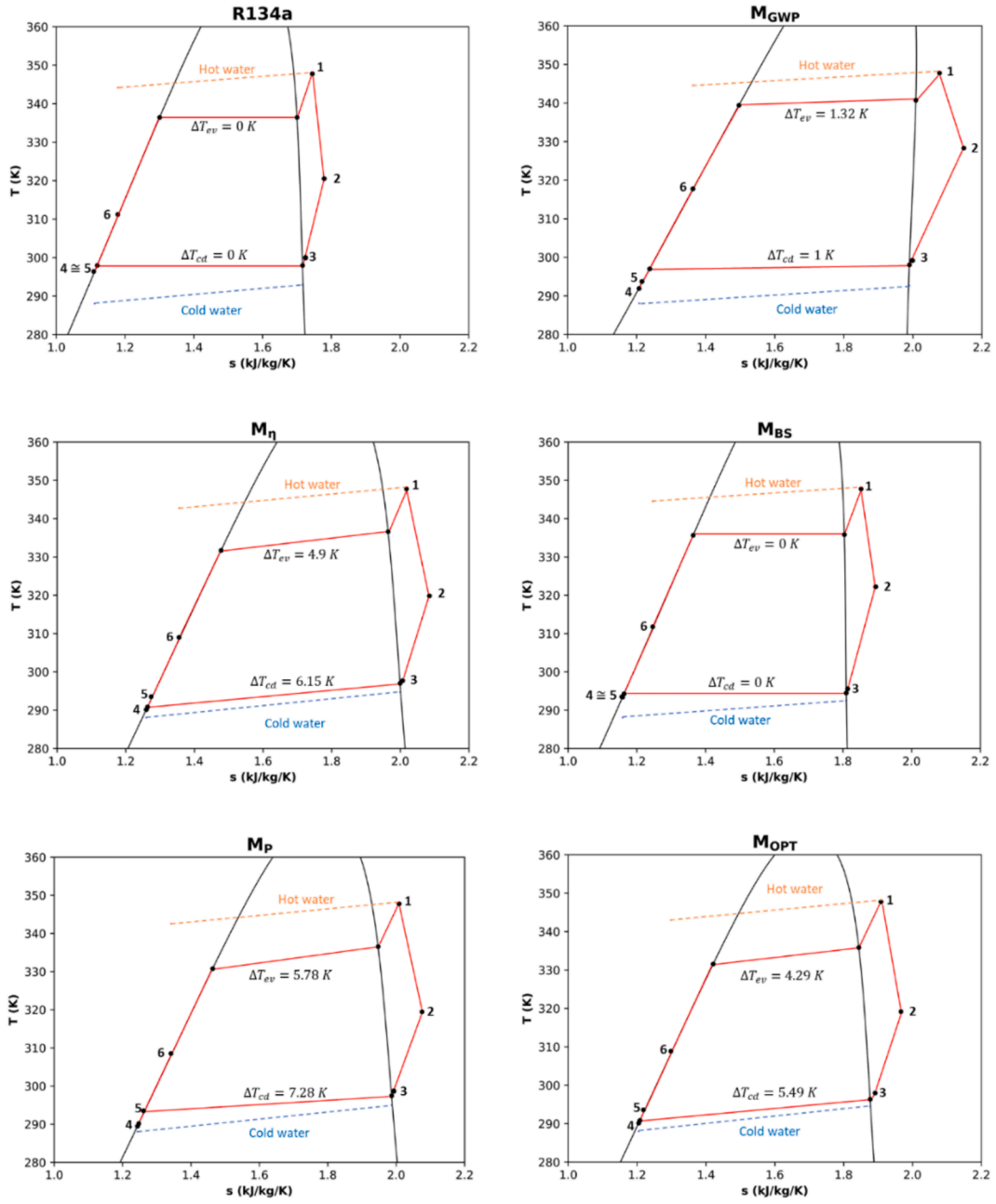

Fig. 13. Temperature-specific entropy diagrams of R134a and the five individual optimal mixtures.

consumption and the expander power output, and is particularly critical with fluids with low critical temperature [46]. To facilitate the comparison, each index in Fig. 12 is normalized by dividing its value by that obtained with R134a. Hence, R134a performance in the radar chart are represented by a regular polygon with vertexes pointed at 1.0. Punctual values of performance indexes and operating conditions are collected in Table 7. Compared to R134a, a substantial increase in the power output and net efficiency is observed for the three mixtures M_η (+77 % and + 25 %, for power and efficiency respectively), M_P (+83 % and + 23 %), M_{OPT} (+62 % and + 19 %). Consistently, such blends present also a modest decrease in the *BWR*, which is in the range between 40 % and 45 %. The other two blends, M_{GWP} and M_{BS}, feature a slight reduction in both power (−16 % and −11 %, for M_{GWP} and M_{BS} respectively) and efficiency (–13 % and −4%). Similar trend is detected for the pump efficiency, whose highest value (close to 35 %) is achieved with the mixture M_{OPT}, with considerable improvement with respect to the value obtained with R134a. None of the optimal mixtures allows to exceed the expander efficiency obtained with R134a, which is close to 36.5 %. However, the penalization of η_{exp} due to the use of the mixtures is limited to few percentage points.

The lowest performance is registered with M_{GWP}, which also presents the highest *BWR* (close to 55 %), and the lowest values of pump and expander efficiency (32 % and 21 % respectively). Table 7 also reports information regarding the working conditions simulated with the ORC model in the operating point selected for the optimization ($T_{H,in} = 75^\circ C$, $T_{C,in} = 15^\circ C$). The analysis of working pressures, flow rates and rotating speeds is fundamental especially in case of retrofit of an existing plant (such as the present case-study), as it provides first indications of the changes on the power plant that may be required to operate with the new fluid. The pump speed remains in the range of rotating speed achievable with the feed-pump of the test bench (90–300 rpm), with the highest values obtained with M_{OPT} (290 rpm) and M_P (275 rpm). Such

Table 8
Fluids environmental (GWP) and safety (flammability class) properties comparison.

FLUIDS	GWP 100y	SAFETY CLASS
R134a	1430	A1 (no flame propagation)
M_{GWP}	5.6	A3 (higher flammability)
M_{η}	518.5	A2L (lower flammability)
M_{BS}	30.3	A2L (lower flammability)
M_P	176.5	A2L (lower flammability)
M_{OPT}	142.1	A2L (lower flammability)

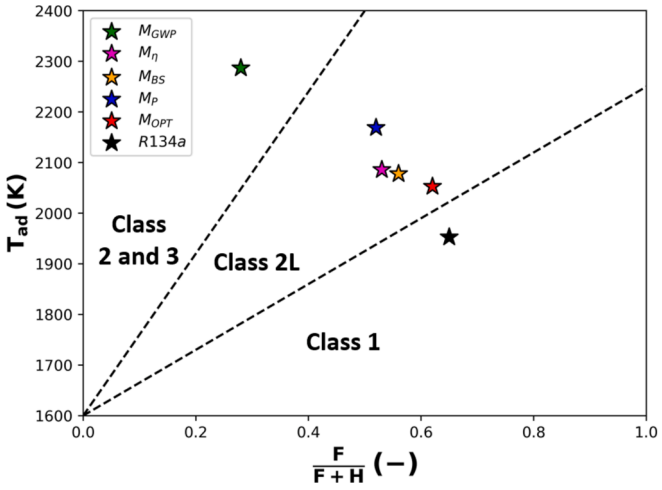

Fig. 14. Flammability class classification (A1, A2L, A2, or A3) shown as a function of T_{ad} and F/(F+H) [49].

conditions suggest that the replacement of the pump is more likely to be considered if these two blends are employed, especially if the system is expected to operate also with higher heat source temperatures. In fact, increasing $T_{H,in}$ the vaporization pressure must increase too, in order to keep the same superheating degree at the expander inlet. Since higher values of p_V are obtained by increasing the fluid mass flow rate –hence the pump speed – the margins of regulation are limited for these two fluids. M_{OPT} and M_P are also the fluids characterized by higher values of vaporization pressure (both around 21 bar), while the lowest values are registered with M_{GWP} (12 bar) and M_{BS} (14.6 bar). The condensation pressure is higher than the ambient pressure for all the six fluids, which allows to avoid the implementation of deaeration systems. The minimum condensation pressure is observed with M_{GWP}, and is close to 4 bar. The values of the expansion ratio (β) for all the optimized blends lie in a limited range (2.75–3.03), and are slightly higher than that of R134a (equal to 2.52). The mixtures M_{OPT}, M_{η} and M_P are zeotropic, with temperatures glides ($\Delta T_{glide} = (T_V - T_L)_{p=const.}$) between 4 K and 7.5 K; the mixture M_{GWP} is near-azeotropic, with a glide lower than 2 K, while the mixture M_{BS} acts as a pure fluid (glide equal to zero). It is worth noting that the mixture M_{OPT} seems very similar to the commercial fluid R457A, a blend made of R32 (18 %), R1234yf (70 %) and R152a (12 %) currently used in HVAC applications as low-GWP replacement for R404A [47].

A graphical comparison of the thermodynamic cycle obtained with each fluid on the temperature-specific entropy diagram is presented in Fig. 13.

3.3. Environmental and safety performance

In assessing the environmental and safety performance of mixtures, the mixing rule outlined in Section 2.1 has been applied to determine the GWP, while the ASHRAE Standard 34 [48] has been used for safety classification (see Table 8).

The toxicity class A is assumed for all the five optimal blends, since all their pure components are classified as low-toxic. The flammability classification was assessed according to the methodology presented in [49], by applying a normalized index that combines the maximum adiabatic flame temperature (T_{ad}) and the number of atoms of fluorine and hydrogen (F/F+H). The adiabatic flame temperature was calculated using the open-source kinetics solver Cantera, and mechanisms available in the literature [50,51,52].

All the mixtures shown in Table 8 ensure a strong GWP reduction (>60 %) compared to that of R134a, with the highest value achieved by M_{η} (close to 520). Mixtures M_{OPT}, M_{BS} and M_{GWP} have GWP lower than 150, which is already the upper limit for some applications in the F-gas regulations [43]. These blends represent the most suitable retrofit options considering long-term scenarios. The lowest value of GWP around 5 is obtained with M_{GWP}, as it is composed by an olefin and i-butane.

Due to the presence of a large fraction of HC, M_{GWP} is also the only mixture that falls in the highest flammability class (A3). The other blends are all classified as low-flammable (A2L) due to the large presence of HFOs. In Fig. 14 the ASHRAE Standard 34 flammability classification (A1, A2L, A2, or A3) is shown as a function of T_{ad} and F/F+H for the five best mixtures and the reference pure fluid R134a.

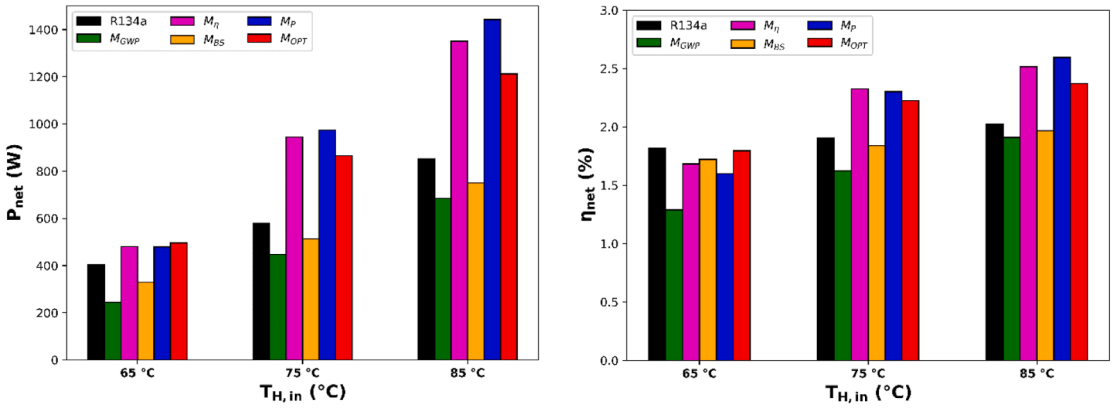

Fig. 15. Performance comparison between the five best solutions and the R134a at three different heat source temperatures: 65, 75, and 85 °C. a: net power output. b:net efficiency.

3.4. Off-design performance

In the final analysis conducted on the five optimal mixtures of Table 7, the ORC model was used to compare the performance metrics (net power and efficiency) of these mixtures and R134a under off-design operating conditions, in particular considering the heat source temperature equal to 65 °C, 75 °C (as in the optimization task) and 85 °C. The outcomes are presented in Fig. 15.

Regarding P_{net}, Fig. 15a reveals that at $T_{H,in}$ equal to 65 °C, the peak power outputs achieved with M_{OPT}, M_P and M_η are remarkably similar. In the cases of $T_{H,in}$ equal to 75 °C and 85 °C instead, the highest value is obtained with M_P (close to 1000 W and 1400 W respectively). In all conditions, the power output with M_{OPT}, M_P and M_η surpasses that of R134a, with the difference becoming more pronounced at higher heat source temperatures. The blends M_{GWP} and M_{BS} shows slightly lower P_{net} values than R134a under all tested conditions.

The findings related to the net efficiency (η_{net}) are depicted in Fig. 15b. The fluid R134a shows the highest efficiency only at a $T_{H,in}$ equal to 65 °C, while at a $T_{H,in}$ of 85 °C the highest value of η_{net} is obtained with M_P. It's important to note that the net efficiency attainable with the reference ORC test rig is low in general (a few percentage points), primarily due to the large impact of pump consumption (high BWR, see Table 7 and [25].

This analysis suggests that, in case the power plant is expected to work under different heat source conditions, the optimization code should be targeted considering multiple operating points. This task can be accomplished, for instance, by running the model under several working conditions and incorporating average performance indexes into the objective function.

4. Applications and limitations of the proposed method

While the methodology has been developed to be adaptable to any specific objective, its application to very different case studies may require some modifications to the settings of the sub-models. The main modifications relate to the blend model and the ORC model, which should be revised according to the specifics of the benchmark case. In particular, the ORC model needs to be replaced by a detailed model of the benchmark case, if available, or by a simplified model based on heat balances and using fixed efficiencies and operating parameters, such as expander and pump efficiencies, superheat and subcooling degrees, pinch point temperature difference, etc. (as the one proposed in [53]). If the global heat transfer coefficient has to be calculated, the correlation for estimating the convective coefficients should be carefully selected according to the fluids considered and the working conditions, as the correlations used here may not be suitable for all ranges of temperature and fluid properties. As far as the optimiser is concerned, minor modifications can be related to the choice of optimisation targets in the objective function and the corresponding weight values and normalisation techniques.

To provide more insights on how the approach can be adapted effectively to different cases, here we would like to propose some examples of potential applications, extremely different from the one presented in this paper as benchmark case:

Example 1: preliminary design of medium-scale ORC system for industrial waste heat recovery.

- Inputs: heat source and cold sink conditions.
- ORC model: simple model in design conditions with fixed parameters.
- Blend model: REFPROP library, equations of state or simple relations (must be verified).
- Optimization targets: net output power, GWP, flammability, heat exchangers surface area, glide.

Example 2: retrofit of refrigeration cycle using low-GWP mixtures.

- Inputs: nominal temperature and cooling capacity, ambient temperature.
- ORC model: detailed model of benchmark refrigeration cycle or simple model in design conditions with fixed parameters.
- Blend model: REFPROP library, equations of state or simple relations (must be verified).
- Optimization targets: Energy Efficiency Ratio (EER), GWP, flammability, heat exchangers surface area.

Example 3: design of a new blend with similar properties to conventional fluid to be replaced.

- Inputs: benchmark fluid's properties.
- ORC model: none.
- Blend model: REFPROP library, equations of state or simple relations (must be verified).
- Optimization targets: specific fluid's properties, GWP, flammability.

It must be noted that the limitation of the number of pure working fluids included in the optimization domain (limited to 20 max) can be overcome by executing multiple runs on different sets of fluids with the same targets. The fluids of each set with highest performance will compose the set for the final optimization. This can be helpful in case the criteria for the pre-screening are not clear at the beginning of a project.

As concluding remark, while using mixtures as working fluids in ORC systems can offer potential benefits in terms of efficiency, environmental impact, and safety compared to pure fluids, there are several practical challenges in mixing and handling these mixtures in real-world settings. There is a lack of literature on this topic, so here we try to summarize some key points related to the main implications related to real use of blends:

- Working fluid mixtures can lead to deterioration in **heat transfer performance**, reducing the real heat transfer coefficients especially during evaporation and condensation [54]. Systems with such mixtures may eventually require larger heat transfer equipment compared to those using single-component working fluids.
- During operation, the **composition** of the working fluid mixture can shift due to selective evaporation of the more volatile component. This can lead to changes in the thermodynamic properties and performance of the ORC system over time [55].
- Many potential mixtures contain flammable components. Proper safety measures and handling procedures are necessary to mitigate the risks associated with flammable fluids in industrial settings [49,22].
- Using mixtures adds **complexity** to the ORC system design, modelling, and optimization. For example, thermal properties may not be available with accuracy. More parameters need to be considered, such as the composition and mixing ratio of the components. Furthermore, there is a limited amount of **experimental data** available on the performance of mixtures in real ORC systems. Most studies have been based on simulations using estimated fluid properties.
- Eventually, the use of mixtures may increase the **initial and operating** costs of the ORC system compared to using pure fluids, due to the need for more complex equipment and additional safety measures.

5. Conclusion

In this paper, a procedure for the design of working fluid mixtures in ORC was developed and tested. The procedure involves three main blocks of functions: the blend model, the system model and the optimizer. These can be tailored to meet specific application objectives. The

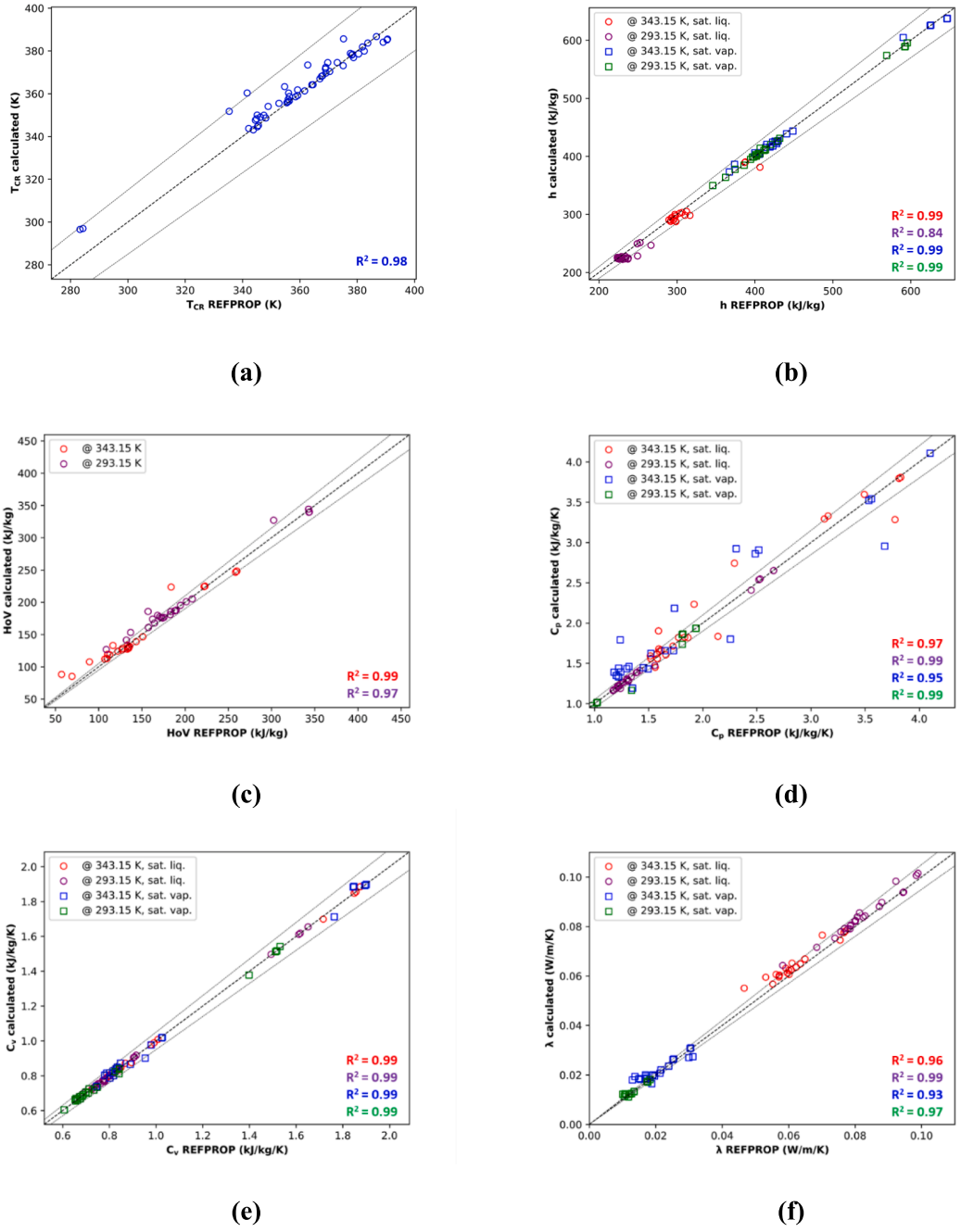

Fig. 16. Parity plot between REFPROP and mixing rules results of: a) critical temperature (T_{CR}), b) specific enthalpy (h), c) latent heat of vaporization (HoV), d) specific heat at constant pressure (C_P), e) specific heat at constant volume (C_V), f) thermal conductivity (λ).

blend model is used to calculate the thermophysical properties of the formulated mixtures. The **ORC system model** applies the mixtures properties to predict their performance in a specific case study, and here is represented by the semi-empirical lumped-parameter model of an experimental ORC test rig. The **optimizer** follows a probabilistic approach, as it employs the Bayesian inference theorem to identify the solution to be analysed. Blend model and ORC model have been validated against Equations of State libraries and experimental data, respectively.

The algorithm capabilities have been tested in a **case study** aimed at replacing the high-GWP fluid HFC-134a in a micro-scale ORC with recuperator. The targets of the case study were to maximize net power output and overall efficiency, and to minimize the GWP and the number of pure fluids composing the blend (BS).

Each optimization target contributes to the value of the objective function, which represents the total "score" of each mixture formulated by the algorithm. A preliminary selection of pure fluids to be mixed is required to define the search domain. The fluid list for the presented case study includes ten substances from different families, specifically HFCs (R134a, R32, R245fa, R227ea, R152a), HFOs (R1234yf, R1234ze(E), R1233zd(E)), and HCs (propane and i-butane), all characterized by critical temperatures close to that of the fluid to be replaced. The safety performance of the designed mixtures has also been estimated, by applying a procedure (available from the literature) to determine the flammability classification of each of the best solutions.

The results show that the most performing mixtures formulated by

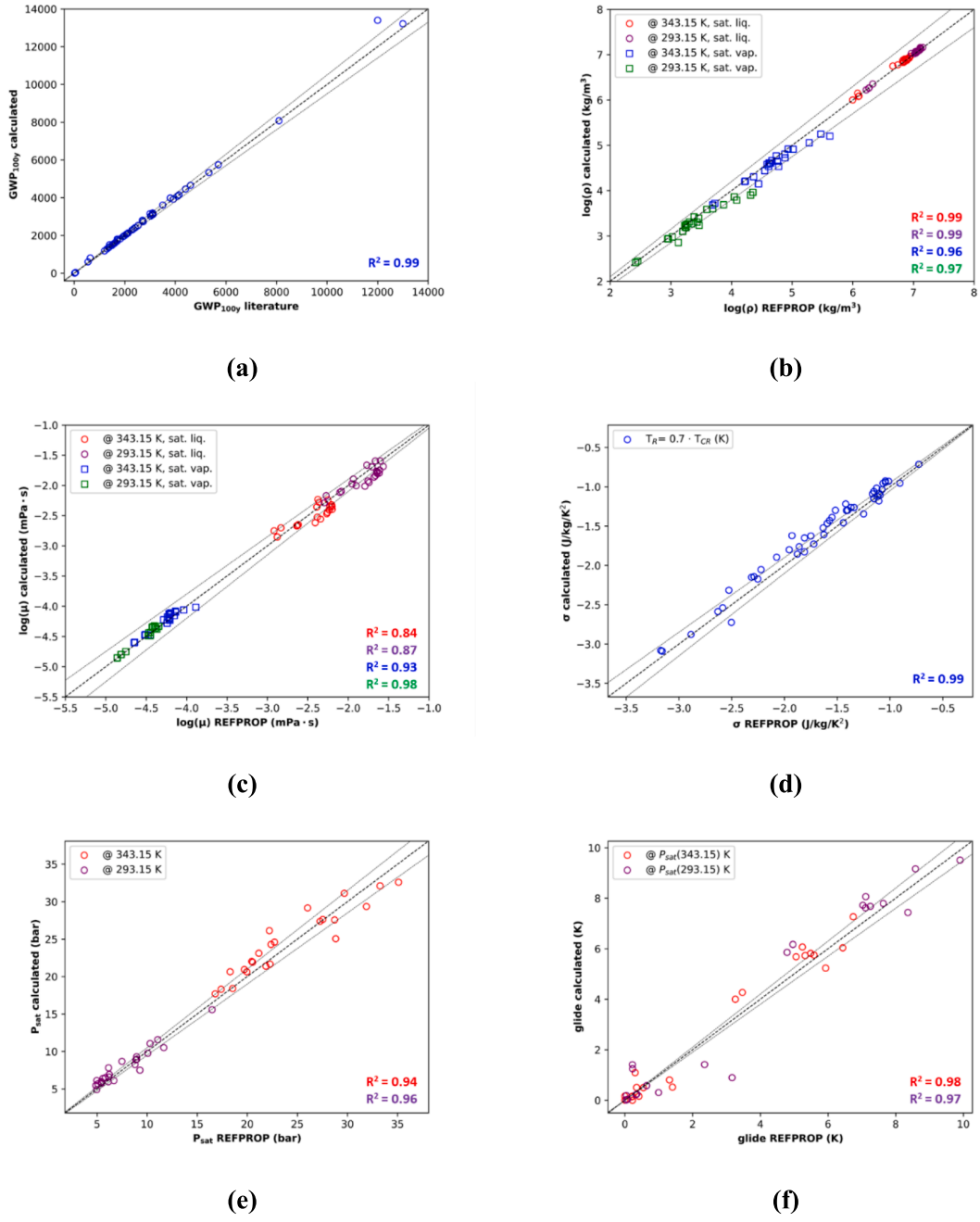

Fig. 17. Parity plot between REFPROP and mixing rules results of: a) GWP, b) density (ρ), c) viscosity (μ), d) molecular complexity (σ), e) saturation pressure (P_{sat}), f) glide.

the algorithm are characterized by a large presence of HFOs and HFCs, with smaller incidence of HCs that are mostly used as GWP-limiter. In particular, the solution with the highest score of the objective function is a ternary blend of R32 (17 %), R1234yf (64 %) and R152a (19 %), which allows an improvement in both net power and efficiency compared to R134a (+62 % and + 19 %, respectively), with a GWP reduction below 150. All the blends composed of HFC and HFO are classified as low flammable (ASHRAE A2L). The best mixture with the lowest GWP value is a blend of isobutane (42 %) and R1234ze(E) (58 %), which however resulted highly flammable (A3). The mixtures related to the highest performance are mostly zeotropic with a glide between 4 K and 7 K.

The working variables simulated with the ORC model, such as the working pressures, flow rate and rotating speeds, remain within a range that is compatible with the conditions achievable by the reference ORC test rig. This is particularly convenient in case of plant retrofitting, as it suggests that only minimal equipment adaptations may be required to operate with the new fluid.

In conclusion, this study introduces a simple yet powerful strategy for designing the optimal mixture in ORC applications. The real advantage of this strategy is its ability to be modified to suit various research and industrial aims, allowing users to adjust the procedure to achieve their unique objectives.

Future developments might be dedicated at increasing the accuracy and applicability of the proposed method. These are some examples for future research activities:

- developing a systematic technique of fluid pre-screening in order to enhance the efficacy of the pre-screening process and to ensure that it is not bonded to case-related criteria that may not be accessible;
- reducing the uncertainty associated with the blend model and ORC model in different applications, especially if the considered set of fluids differ substantially from those of the case study presented in this work; this would mean to provide mixing rules that ensure accuracy in estimating mixture properties and adjusted correlations and coefficients for assessing the heat transfer properties;
- performing experimental tests with binary and tertiary mixtures for acquiring experimental data to validate the mixing rules and the models, and for providing information on practical issues within real-world settings.

Declaration of Generative AI and AI-assisted technologies in the writing process

During the preparation of this work the authors used AI-based tools, specifically Microsoft Copilot and OpenAI's ChatGPT, in order to assist in language editing. After using these tools, the authors reviewed and edited the content as needed and take full responsibility for the content of the publication.

CRediT authorship contribution statement

Valerio Mariani: Writing – review & editing, Writing – original draft, Methodology, Conceptualization. **Saverio Ottaviano:** Writing – review & editing, Writing – original draft, Methodology, Conceptualization. **Davide Scampamorte:** Writing – original draft, Software, Formal analysis. **Andrea De Pascale:** Writing – review & editing, Supervision, Conceptualization. **Giulio Cazzoli:** Software, Methodology. **Lisa Branchini:** Supervision, Project administration. **Gian Marco Bianchi:** Supervision, Project administration.

Declaration of competing interest

The authors declare that they have no known competing financial interests or personal relationships that could have appeared to influence the work reported in this paper.

Acknowledgements

- This study was carried out within the NEST - Network 4 Energy Sustainable Transition (D.D. 1243 02/08/2022, PE00000021) and received funding under the National Recovery and Resilience Plan (NRRP), Mission 4 Component 2 Investment 1.3, funded from the European Union - NextGenerationEU. This manuscript reflects only the authors' views and opinions, neither the European Union nor the European Commission can be considered responsible for them.
- This research project originated from a collaboration started in 2021 between the group "Fluid Machines and Energy Systems" and the group "Development and simulation of low-impact internal combustion engines" of the University of Bologna.

Appendix

Mixing rules validation

References

[1] Wieland C, Schifflechner C, Dawo F, Astolfi M. The organic Rankine cycle power systems market: Recent developments and future perspectives. Appl Therm Eng Apr. 2023;224:119980. https://doi.org/10.1016/j.applthermaleng.2023.119980.

[2] Bianchi G, Panayiotou G, Aresti L, Kalogirou SA, Florides GA, Tsamos K, et al. Estimating the waste heat recovery in the European Union Industry. Energy Ecol Environ Oct. 2019;4(5):211–21. https://doi.org/10.1007/s40974-019-00132-7.

[3] E. Macchi and M. Astolfi, *Organic Rankine Cycle (ORC) Power Systems: Technologies and Applications*. Elsevier Inc., 2016. Accessed: Sep. 24, 2024. [Online]. Available: https://re.public.polimi.it/handle/11311/1048398.

[4] Oyewunmi OA, Kirmse CJW, Pantaleo AM, Markides CN. Performance of working-fluid mixtures in ORC-CHP systems for different heat-demand segments and heat-recovery temperature levels. Energy Convers Manag Sep. 2017;148:1508–24. https://doi.org/10.1016/j.enconman.2017.05.078.

[5] G. Angelino and P. Colonnadipaliano, 'Multicomponent Working Fluids For Organic Rankine Cycles (ORCs)', *Energy*, vol. 23, no. 6, Art. no. 6, Jun. 1998, doi: 10.1016/S0360-5442(98)00009-7.

[6] Advantages and issues'. G. Bamorovat Abadi and K. C. Kim, 'Investigation of organic Rankine cycles with zeotropic mixtures as a working fluid. Renew Sustain Energy Rev Jun. 2017;73:1000–13. https://doi.org/10.1016/j.rser.2017.02.020.

[7] Braimakis K, Mikelis A, Charalampidis A, Karellas S. Exergetic performance of CO2 and ultra-low GWP refrigerant mixtures as working fluids in ORC for waste heat recovery. Energy Jul. 2020;203:117801. https://doi.org/10.1016/j.energy.2020.117801.

[8] Shu G, Gao Y, Tian H, Wei H, Liang X. Study of mixtures based on hydrocarbons used in ORC (Organic Rankine Cycle) for engine waste heat recovery. Energy Sep. 2014;74:428–38. https://doi.org/10.1016/j.energy.2014.07.007.

[9] Lin M-H, Tsai J-F, Yu C-S. A Review of Deterministic Optimization Methods in Engineering and Management. Math Probl Eng 2012;2012(1):756023. https://doi.org/10.1155/2012/756023.

[10] V. Kumar and S. M. Yadav, 'A state-of-the-Art review of heuristic and metaheuristic optimization techniques for the management of water resources', *Water Supply*, vol. 22, no. 4, Art. no. 4, Apr. 2022, doi: 10.2166/ws.2022.010.

[11] Spall JC. Stochastic Optimization. In: Gentle JE, Härdle WK, Mori Y, editors. Handbook of Computational Statistics: Concepts and Methods. Berlin, Heidelberg: Springer; 2012. p. 173–201. https://doi.org/10.1007/978-3-642-21551-3_7.

[12] Freeman J, Hellgardt K, Markides CN. Working fluid selection and electrical performance optimisation of a domestic solar-ORC combined heat and power system for year-round operation in the UK. Appl Energy Jan. 2017;186:291–303. https://doi.org/10.1016/j.apenergy.2016.04.041.

[13] White MT, Oyewunmi OA, Chatzopoulou MA, Pantaleo AM, Haslam AJ, Markides CN. Computer-aided working-fluid design, thermodynamic optimisation and thermoeconomic assessment of ORC systems for waste-heat recovery. Energy Oct. 2018;161:1181–98. https://doi.org/10.1016/j.energy.2018.07.098.

[14] Schilling J, Entrup M, Hopp M, Gross J, Bardow A. Towards optimal mixtures of working fluids: Integrated design of processes and mixtures for Organic Rankine Cycles. Renew Sustain Energy Rev Jan. 2021;135:110179. https://doi.org/10.1016/j.rser.2020.110179.

[15] Chen C, Su W, Yu A, Lin X, Zhou N. Combining cubic equations with group contribution methods to predict cycle performances and design working fluids for four different organic Rankine cycles. Energy Convers Manag X Aug. 2022;15:100245. https://doi.org/10.1016/j.ecmx.2022.100245.

[16] Cignitti S, Andreasen JG, Haglind F, Woodley JM, Abildskov J. Integrated working fluid-thermodynamic cycle design of organic Rankine cycle power systems for waste heat recovery. Appl Energy Oct. 2017;203:442–53. https://doi.org/10.1016/j.apenergy.2017.06.031.

[17] A. K. Sleiti and W. A. Al-Ammari, 'Systematic thermodynamic approach for designing mixed refrigerants used in hydrogen precooling process', *Int. J. Hydrog. Energy*, vol. 47, no. 48, Art. no. 48, Jun. 2022, doi: 10.1016/j.ijhydene.2022.04.233.

[18] M. Lampe, M. Stavrou, H. M. Bücker, J. Gross, and A. Bardow, 'Simultaneous Optimization of Working Fluid and Process for Organic Rankine Cycles Using PC-SAFT', *Ind. Eng. Chem. Res.*, vol. 53, no. 21, Art. no. 21, May 2014, doi: 10.1021/ie5006542.

[19] Chitgar N, Hemmati A, Sadrzadeh M. A comparative performance analysis, working fluid selection, and machine learning optimization of ORC systems driven by geothermal energy. Energy Convers Manag Jun. 2023;286:117072. https://doi.org/10.1016/j.enconman.2023.117072.

[20] A. I. Papadopoulos, M. Stijepovic, and P. Linke, 'On the systematic design and selection of optimal working fluids for Organic Rankine Cycles', *Appl. Therm. Eng.*, vol. 30, no. 6–7, Art. no. 6–7, May 2010, doi: 10.1016/j.applthermaleng.2009.12.006.

[21] Fang Y, Yang F, Zhang H. Comparative analysis and multi-objective optimization of organic Rankine cycle (ORC) using pure working fluids and their zeotropic mixtures for diesel engine waste heat recovery. Appl Therm Eng Jul. 2019;157:113704. https://doi.org/10.1016/j.applthermaleng.2019.04.114.

[22] Li Z, Shen B, Gluesenkamp KR. Multi-objective optimization of low-GWP mixture composition and heat exchanger circuitry configuration for improved system performance and reduced refrigerant flammability. Int J Refrig Jun. 2021;126:133–42. https://doi.org/10.1016/j.ijrefrig.2021.01.003.

[23] Díaz-Secades LA, González R, Rivera N, Quevedo JR, Montañés E. Parametric study of organic Rankine working fluids via Bayesian optimization of a preference learning ranking for a waste heat recovery system applied to a case study marine engine. Ocean Eng Aug. 2024;306:118124. https://doi.org/10.1016/j.oceaneng.2024.118124.

[24] Stigler SM. Thomas Bayes's Bayesian Inference. J r Stat Soc Ser Gen 1982;145(2):250–8. https://doi.org/10.2307/2981538.

[25] Bianchi M, Branchini L, Casari N, De Pascale A, Melino F, Ottaviano S, et al. Experimental analysis of a micro-ORC driven by piston expander for low-grade heat recovery. Appl Therm Eng Feb. 2019;148:1278–91. https://doi.org/10.1016/j.applthermaleng.2018.12.019.

[26] V. Mariani, L. Pulga, G. M. Bianchi, S. Falfari, and C. Forte, 'Machine Learning-Based Identification Strategy of Fuel Surrogates for the CFD Simulation of Stratified

Operations in Low Temperature Combustion Modes', *Energies*, vol. 14, no. 15, Art. no. 15, Jan. 2021, doi: 10.3390/en14154623.
[27] Bianchi M, Branchini L, De Pascale A, Melino F, Ottaviano S, Peretto A, et al. Performance and total warming impact assessment of pure fluids and mixtures replacing HFCs in micro-ORC energy systems. Appl Therm Eng Feb. 2022;203: 117888. https://doi.org/10.1016/j.applthermaleng.2021.117888.
[28] Mariani V, Ottaviano S, De Pascale A, Cazzoli G, Branchini L, Bianchi GM. Guidelines and optimization criteria of a machine learning-based methodology for mixture design in ORC systems. ESP 2023. https://doi.org/10.12795/9788447227457_41.
[29] 'High-Level Interface — CoolProp 6.4.3 documentation'. Accessed: Jul. 03, 2023. [Online]. Available: http://www.coolprop.org/coolprop/HighLevelAPI.html.
[30] L. Grunberg and A. H. Nissan, 'Mixture Law for Viscosity', *Nature*, vol. 164, no. 4175, Art. no. 4175, Nov. 1949, doi: 10.1038/164799b0.
[31] Soave G. Equilibrium constants from a modified Redlich-Kwong equation of state. Chem Eng Sci Jun. 1972;27(6):1197–203. https://doi.org/10.1016/0009-2509(72)80096-4.
[32] 'W-refrigerant' Accessed: Aug. 24, 2023. [Online]. Available: https://w-refrigerant.com/en/technology-en/tables/.
[33] Ottaviano S, Poletto C, Ancona MA, Melino F. Experimental investigation on micro-ORC system operating with partial evaporation and two–phase expansion. Energy Convers Manag Dec. 2022;274:116415. https://doi.org/10.1016/j.enconman.2022.116415.
[34] J. P. Holman, *Heat Transfer*. in McGraw-Hill series in mechanical engineering. McGraw-Hill, 2002. [Online]. Available: https://books.google.it/books?id=M3wpAQAAMAAJ.
[35] W. Kays, M. Crawford, and B. Weigand, 'CONVECTIVE HEAT AND MASS TRANSFER', *Convect. Heat Mass Transf.*.
[36] Giuffrida A. Modelling the performance of a scroll expander for small organic Rankine cycles when changing the working fluid. Appl Therm Eng Sep. 2014;70(1): 1040–9. https://doi.org/10.1016/j.applthermaleng.2014.06.004.
[37] Bianchi M, Branchini L, De Pascale A, Melino F, Ottaviano S, Peretto A, et al. Replacement of R134a with low-GWP fluids in a kW-size reciprocating piston expander: Performance prediction and design optimization. Energy Sep. 2020;206: 118174. https://doi.org/10.1016/j.energy.2020.118174.
[38] Y. Glavatskaya, P. Podevin, V. Lemort, O. Shonda, and G. Descombes, 'Reciprocating Expander for an Exhaust Heat Recovery Rankine Cycle for a Passenger Car Application', *Energies*, vol. 5, no. 6, Art. no. 6, Jun. 2012, doi: 10.3390/en5061751.
[39] Shahriari B, Swersky K, Wang Z, Adams RP, de Freitas N. Taking the Human Out of the Loop: A Review of Bayesian Optimization. Proc IEEE Jan. 2016;104(1):148–75. https://doi.org/10.1109/JPROC.2015.2494218.
[40] *Bayesian Optimization*. (Dec. 13, 2023). Python. bayesian-optimization. Accessed: Dec. 13, 2023. [Online]. Available: https://github.com/bayesian-optimization/BayesianOptimization.
[41] S. Rana, C. Li, S. Gupta, V. Nguyen, and S. Venkatesh, 'High Dimensional Bayesian Optimization with Elastic Gaussian Process', in *Proceedings of the 34th International Conference on Machine Learning*, PMLR, Jul. 2017, pp. 2883–2891. Accessed: Jun. 03, 2024. [Online]. Available: https://proceedings.mlr.press/v70/rana17a.html.
[42] 'AR4 Climate Change 2007: Synthesis Report — IPCC'. Accessed: Mar. 14, 2024. [Online]. Available: https://www.ipcc.ch/report/ar4/syr/.
[43] Radley-Gardner O, Beale H, Zimmermann R. Eds., *Fundamental Texts On European Private Law*. Hart Publishing 2016. https://doi.org/10.5040/9781782258674.
[44] 'tf.keras.Regularizer | TensorFlow v2.16.1', TensorFlow. Accessed: Jun. 03, 2024. [Online]. Available: https://www.tensorflow.org/api_docs/python/tf/keras/Regularizer.
[45] Bahrami M, Pourfayaz F, Kasaeian A. Low global warming potential (GWP) working fluids (WFs) for Organic Rankine Cycle (ORC) applications. Energy Rep Nov. 2022;8:2976–88. https://doi.org/10.1016/j.egyr.2022.01.222.
[46] Quoilin S, Broek MVD, Declaye S, Dewallef P, Lemort V. Techno-economic survey of Organic Rankine Cycle (ORC) systems. Renew Sustain Energy Rev Jun. 2013;22: 168–86. https://doi.org/10.1016/j.rser.2013.01.028.
[47] Llopis R, Calleja-Anta D, Sánchez D, Nebot-Andrés L, Catalán-Gil J, Cabello R. R-454C, R-459B, R-457A and R-455A as low-GWP replacements of R-404A: Experimental evaluation and optimization. Int J Refrig Oct. 2019;106:133–43. https://doi.org/10.1016/j.ijrefrig.2019.06.013.
[48] 'ANSI/ASHRAE Addendum f to ANSI/ASHRAE Standard 34-2019'.
[49] Bell IH, Domanski PA, McLinden MO, Linteris GT. The hunt for nonflammable refrigerant blends to replace R-134a. Int J Refrig Aug. 2019;104:484–95. https://doi.org/10.1016/j.ijrefrig.2019.05.035.
[50] Linteris G, Babushok V. Laminar burning velocity predictions for C1 and C2 hydrofluorocarbon refrigerants with air. J Fluor Chem Feb. 2020;230:109324. https://doi.org/10.1016/j.jfluchem.2019.05.002.
[51] Needham CD, Westmoreland PR. Combustion and flammability chemistry for the refrigerant HFO-1234yf (2,3,3,3-tetrafluoropropene). Combust Flame Oct. 2017; 184:176–85. https://doi.org/10.1016/j.combustflame.2017.06.004.
[52] Babushok VI, Linteris GT. Kinetic mechanism of 2,3,3,3-tetrafluoropropene (HFO-1234yf) combustion. J Fluor Chem Sep. 2017;201:15–8. https://doi.org/10.1016/j.jfluchem.2017.07.005.
[53] 'pocketORC | Martin White'. Accessed: Sep. 23, 2024. [Online]. Available: https://martintwhite.github.io/pocketORC/.
[54] Dorao CA, Fernandino M. On the heat transfer deterioration during condensation of binary mixtures. Appl Phys Lett May 2019;114(17):171902. https://doi.org/10.1063/1.5086738.
[55] Krempus D, Bahamonde S, van der Stelt TP, Klink W, Colonna P, De Servi CM. On mixtures as working fluids of air-cooled ORC bottoming power plants of gas turbines. Appl Therm Eng Jan. 2024;236:121730. https://doi.org/10.1016/j.applthermaleng.2023.121730.